nature chemical biology

ARTICLES

https://doi.org/10.1038/s41589-022-01117-0

Structural basis for activation of fungal sterol receptor Upc2 and azole resistance

Lingchen Tan, Lin Chen, Huiseon Yang, Binghui Jin, Gyudong Kim and Young Jun Im ✉

Fungal transcription factor Upc2 senses ergosterol levels and regulates sterol biosynthesis and uptake. Constitutive activation of Upc2 causes azole resistance in *Candida* species. We determined the structure of ergosterol-bound Upc2, revealing the ligand specificity and transcriptional regulation. Ergosterol binding involves conformational changes of the ligand-binding domain, creating a shape-complementary hydrophobic pocket. The conserved helix α12 and glycine-rich loop are critical for sterol recognition by forming the pocket wall. The mutations of the glycine-rich loop inhibit ligand binding by steric clashes and constitutively activate Upc2. The translocation of Upc2 is regulated by Hsp90 chaperone in a sterol-dependent manner. Ergosterol-bound Upc2 associates with Hsp90 using the C-terminal tail, which retains the inactive Upc2 in the cytosol. Ergosterol dissociation induces a conformational change of the C-terminal tail, releasing Upc2 from Hsp90 for nuclear transport by importin α. The understanding of the regulatory mechanism provides an antifungal target for the treatment of azole-resistant *Candida* infections.

Sensing the cellular ergosterol level and regulating sterol biosynthesis and uptake are critical for fungal lipid homeostasis. Within the Saccharomycotina subphylum including *Saccharomyces cerevisiae*, a zinc cluster transcription factor, Upc2 (sterol uptake control protein 2) regulates the transcription of the sterol-related genes[1]. Owing to the essential role of ergosterol in fungal membranes, a majority of antifungal agents target enzymes in ergosterol biosynthetic pathways[2]. The azoles widely used for the treatment of *Candida* infections deplete ergosterol and accumulate toxic sterol precursors by inhibiting lanosterol 14α-demethylase (*ERG11*), resulting in growth inhibition[3,4]. Resistance of *Candida* species to azoles frequently appears in patients with long-term azole therapy by multiple mechanisms. The resistance can be acquired by the mutation of *ERG11* gene, increased expression of the target gene and drug efflux pumps, and biofilm formation[5,6].

Upc2 controls the transcriptional activation of sterol biosynthesis in the pathogenic *Candida* species[7–10]. Upc2 contains an N-terminal nuclear localization signal (NLS) followed by a DNA-binding zinc cluster domain and the C-terminal ligand-binding domain (LBD)[11]. When bound with ergosterol, Upc2 is retained in the cytosol with a transcriptionally inactive conformation. Upc2 has a canonical bipartite NLS, and the ligand-free Upc2 is transported to the nucleus by importin α. Upon ergosterol depletion by azole treatment, the dissociation of ergosterol from Upc2 causes its translocation to the nucleus, where it activates the transcription of sterol biosynthesis and uptake genes[8,11–13]. Therefore, *UPC2*-activating mutations contribute to azole resistance, whereas disruption of *UPC2* increases azole susceptibility[14]. Mutations in the C-terminal glycine-rich loop abolish the sterol binding and make Upc2 constitutively active, which leads to azole resistance in *S. cerevisiae* and *C. albicans*[11,15–18]. The reported structure of apo *S. cerevisiae* Upc2 (hereafter, *Sc*Upc2) LBD lacked a cavity to accommodate a sterol molecule, suggesting ligand binding involves a substantial conformational change[11]. The ligand specificity of Upc2 was elusive owing to the lack of structural information on the ergosterol-bound Upc2. In addition, the determinant for the cytosolic retention of the inactive Upc2 was unknown, obscuring the mechanism of Upc2 translocation.

Hsp90 is an essential and conserved molecular chaperone in eukaryotes that assists the folding of diverse proteins. Hsp90 has an ATPase activity coupled to its chaperone function with a series of conformational changes[19]. Hsp90 interacts dynamically with its client proteins, modulating their stability and activities in response to environmental conditions[20]. Mammalian Hsp90 binds directly to the LBDs of glucocorticoid receptor (GR) and estrogen receptor, and the complexes reside in the cytosol[21]. Hsp90 keeps the receptors inactive until they bind the proper steroid ligands[20]. Ligand binding to the GR causes the dissociation of Hsp90 from the receptor and provokes the receptor to bind DNA[22]. Mapping the Hsp90 genetic interaction network in *C. albicans* identified numerous transcription factors, including Upc2 (ref. [23]). In addition, the Hsp90-mediated morphogenesis of *C. albicans* occurs via Upc2, implying the regulatory role of Hsp90 on Upc2 activity[24].

In this study, we determined the structures of the inactivated Upc2 LBDs in ergosterol-bound forms. Upc2 binds ergosterol in a deep cavity, which involves a large conformational change in the Upc2 LBD. The structure explains how the mutations in the glycine-rich loop inhibit ligand binding and lead to constitutive activation. In addition, we discovered a regulatory role of the molecular chaperone Hsp90 in Upc2 translocation. The overall regulation mechanism of Upc2 by a sterol ligand and Hsp90 shows a similarity to metazoan steroid receptors with an inverse mode of activation. Our results demonstrate that fungi harbor a nuclear receptor-like pathway controlling sterol biosynthesis and azole resistance, representing a co-therapeutic target for the treatment of *Candida* infections.

Results

Structure of the ergosterol-bound Upc2. *Candida glabrata* Upc2A (hereafter denoted as *Cg*Upc2) contains an NLS and a $Zn(II)_2Cys_6$ cluster DNA-binding domain (DBD) in the N-terminal region (Fig. 1a and Extended Data Fig. 1a). The long middle region (residues 82–620) is predicted as disorder loops and is variable in sequence among Upc2 homologs. The C-terminal region contains a conserved LBD with a typical size of 300 residues. All Upc2

College of Pharmacy, Chonnam National University, Gwangju, South Korea. ✉e-mail: imyoungjun@jnu.ac.kr

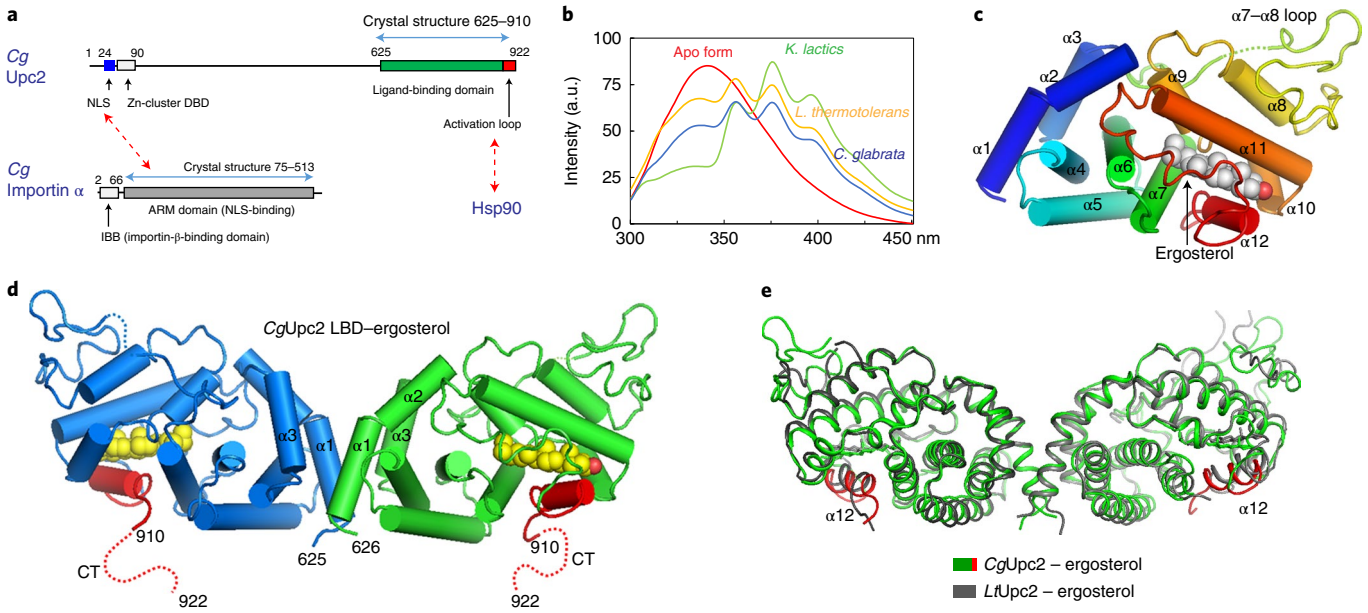

Fig. 1 | The structures of the ergosterol-bound Upc2 LBDs. a, Schematic representation of the domain structures of *Cg*Upc2 and *Cg*Impα. Red dotted lines indicate protein–protein interaction. **b**, Sterol-binding activities of the Upc2 LBDs from several fungal species including *K. lactics*, *L. thermotolerans*, and *C. glabrata*. DHE-binding activity was examined by monitoring fluorescence spectra upon excitation at 285 nm after incubating the recombinant proteins with DOPC:DHE (90:10 molar ratio) liposomes. The spectral measurements were repeated two times, and the representative data were shown. a.u., arbitrary units. **c**, The monomer structure of the *Cg*Upc2 LBD. The structure is colored along with the N to C terminus in blue to red colors. The disordered residues in the α7–α8 loop were shown in dotted lines. **d**, Overall structure of the ergosterol-bound *Cg*Upc2 LBD. The dimeric structure of *Cg*Upc2 LBD was shown in cylindrical representation with bound ergosterol in the sphere model. The C-terminal helix α12 is colored in red. The disordered C-terminal tail (residue 911–922), also known as the 'activation loop' was invisible in the crystal structure and indicated by dotted lines. **e**, Structural comparison of the ergosterol-bound Upc2 LBDs from *C. glabrata* and *L. thermotolerans*.

homologs have a conserved loop at the C termini of the LBDs with a length of 13–17 residues (Extended Data Fig. 1b). The C-terminal tail (CT) connected to the preceding α12 by three glycine residues contains conserved patches of hydrophobic residues.

We purified the LBDs of the Upc2 homologs from *K. lactics*, *C. glabrata*, and *L. thermotolerance*, and confirmed their sterol-binding activities (Fig. 1b). Dehydroergosterol (DHE) is a natural fungal sterol with intrinsic fluorescence properties[25]. Tryptophan residues of the Upc2 LBDs were excited at 285 nm, and the fluorescence spectrum was monitored. Incubation of the Upc2 LBDs with 1,2-dioleoyl-*sn*-glycero-3-phosphocholine (DOPC):DHE liposomes resulted in tryptophan quenching at 340 nm and the appearance of emission peaks at 354, 373, and 393 nm by the fluorescence resonance energy transfer (FRET) from the LBD to the bound DHE (Fig. 1b). We determined the crystal structures of *Cg*Upc2 LBD (residues 621–922) and *L. thermotolerance* Upc2 (hereafter, *Lt*Upc2) LBD (residues 471–788) in ergosterol-bound forms (Supplementary Table 1 and Extended Data Fig. 2). The structure of the ergosterol-bound *Cg*Upc2 LBD displays a globular α-helical-fold composed of 12 α-helices (Fig. 1c,d). The C-terminal half of the LBDs has six α-helices and several flexible loops. The helix α12 is connected to the upstream and downstream residues by the conserved poly-glycine loops. The CTs following the α12 in *Cg*Upc2 and *Lt*Upc2 LBDs were disordered and not visible (Extended Data Fig. 3). The monomer structures of *Cg*Upc2 and *Lt*Upc2 LBDs were highly similar with a C_α root-mean-square deviation of 0.93 Å except for the variable α7–α8 loops (Fig. 1e). The LBDs of *Cg*Upc2 and *Lt*Upc2 were constitutive dimers in solution regardless of the ligand-binding state. The Upc2 LBDs from *Sc*Upc2, *Cg*Upc2, and *Lt*Upc2 have conserved dimeric configurations with the dimer interface formed by α1 and α3.

Ergosterol binds to the hydrophobic tunnel formed by the C-terminal half of the LBD. Ergosterol is buried in the pocket except for the 3-hydroxyl group oriented toward the surface (Fig. 2a). The binding pocket surrounded by six α-helices is composed of entirely hydrophobic residues except for two hydrophilic atoms. The 3-hydroxyl group of sterol makes a hydrogen bond with Arg859 of α10 (Arg722 in *Lt*Upc2) at the tunnel entrance (Fig. 2b). The hydrocarbon rings of ergosterol contact the 12 conserved hydrophobic residues, including the five methionine residues of α11 and α12 (Extended Data Fig. 1b). The hydrophobic cavity of Upc2 is shape complementary to ergosterol. The pocket accommodating hydrocarbon rings of sterol is conserved, while the pocket holding the sterol side chain is variable in *Cg*Upc2 and *Lt*Upc2 (Fig. 2c). The different shapes of sterol-binding pockets of *Cg*Upc2 and *Lt*Upc2 are caused by a variation of Val750 (Ala613 for *Lt*Upc2) and a slightly loose closure of α12 in *Lt*Upc2 (Fig. 2d). The cavity volumes of *Cg*Upc2 and *Lt*Upc2 are 554 and 620 Å^3, respectively, which hold an ergosterol molecule with the volume of 427.3 Å^3. Solvent molecules are excluded from the cavities in the sterol-bound Upc2 LBDs. Despite the slight variation of the sub-pockets, the orientations of the bound ergosterol are identical in *Cg*Upc2 and *Lt*Upc2 LBDs (Fig. 2d). The L847F mutation in the cavity contacting the hydrocarbon rings completely abolished the DHE binding (Fig. 2e). However, V746L or L865F in the cavity accommodating the sterol side chain did not abolish DHE binding, which correlates with the shape variation of the sub-pockets in Upc2 homologs. We observed the consistent DHE-binding properties of these mutants (L837F, V736L, and L855F) in the *Sc*Upc2 LBD (Extended Data Fig. 4a–c).

The azole-resistant clinical isolates of *C. albicans* were reported to contain mutations in the glycine-rich loop of Upc2 (ref. [18]) (Fig. 2b and Extended Data Fig. 1b). The mutation of Gly898 (Gly888

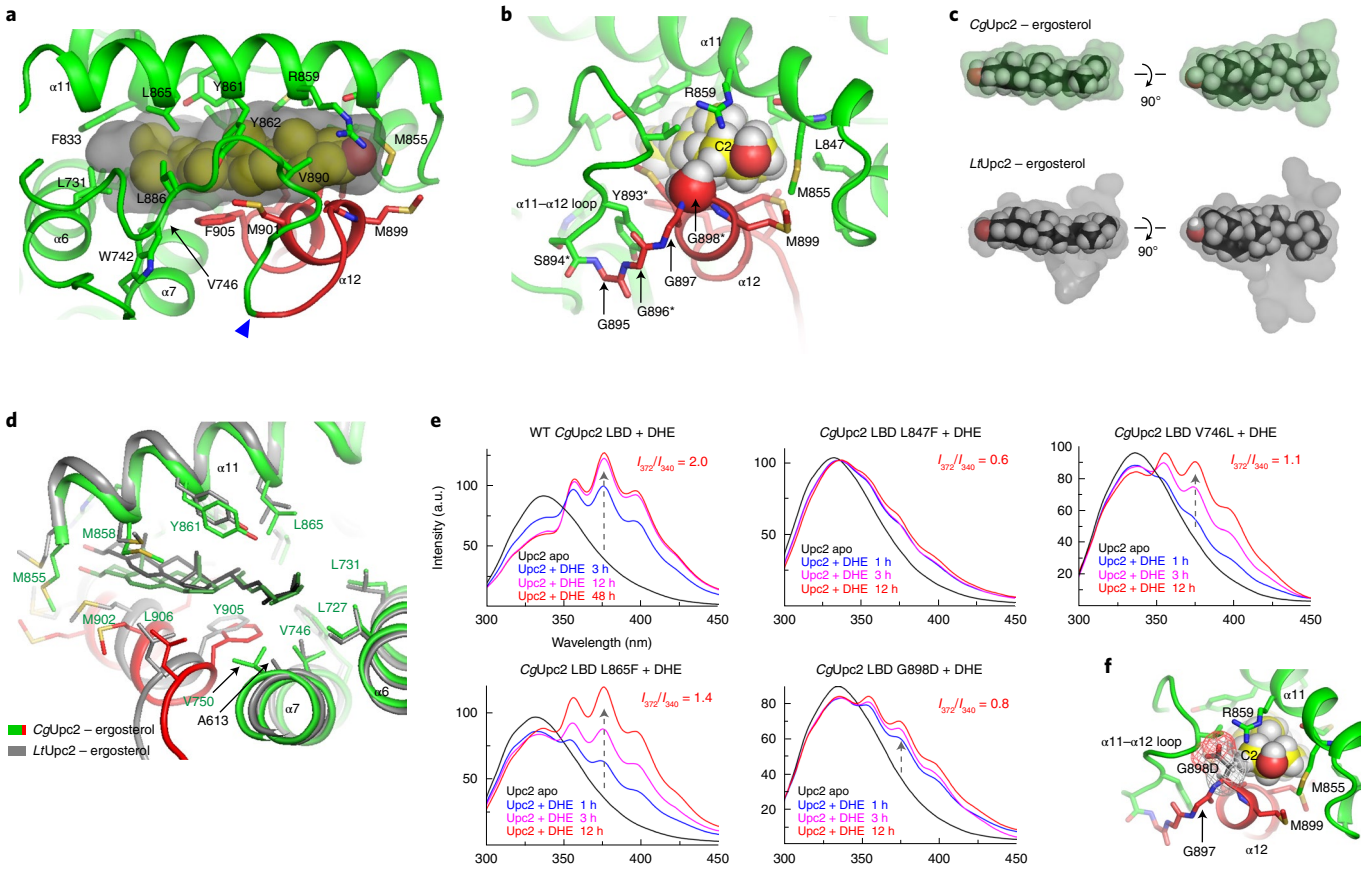

Fig. 2 | The ergosterol-binding pockets of the Upc2 LBDs. a, Sterol-binding pocket of the *Cg*Upc2 LBD. The residues contacting with ergosterol are shown in stick models. The sterol-binding cavity is shown as a transparent surface. The helix α12 composing the hydrophobic wall of the ligand-binding pocket is shown in red. The blue triangle indicates the insertion site of the thrombin cleavage sequence for protease susceptibility assay. **b**, The C_α atom of Gly898 in the glycine-rich loop (α11–α12) contacts with the C2 atom of ergosterol. The *UPC2* gain-of-function mutations identified in the clinical isolates of fluconazole-resistant *C. albicans*[18] are indicated by asterisks. **c**, Comparison of sterol-binding cavities of the *Cg*Upc2 and *Lt*Upc2 LBDs. The binding cavities are shown in transparent surfaces, and the ergosterol molecules were in sphere models. **d**, Comparison of the sterol-binding sites of the *Cg*Upc2 and *Lt*Upc2 LBDs. The side chains of the residues contacting with sterol were shown in stick models. **e**, Sterol-binding assay of the wild-type *Cg*Upc2 LBD and mutants. The DHE binding was monitored by changes in fluorescence spectra with an excitation wavelength of 285 nm. The intensity ratio I_{372}/I_{340} reflects the extent of FRET between Upc2 and DHE. Apo Upc2 has 0.4, and the Upc2 LBD saturated with DHE shows 2.0 for the I_{372}/I_{340} values. We have indicated the maximum I_{372}/I_{340} values for the LBD binding-site mutants. The spectral measurements were repeated two times with consistent results, and the representative data were shown.

in *Sc*Upc2) to any other residues resulted in constitutive activation of Upc2 (ref. [9]). The G898D mutation in *Cg*Upc2 LBD inhibited the sterol binding (Fig. 2e). The C_α atom of Gly898 directly contacts the C2 atom of ergosterol. The modeling of G898D shows that the side chain clashes with the sterol C2 atom and the α11–α12 loop, which interferes with the ligand binding and the closed conformation of α12 (Fig. 2f). The steric clashes explain why any mutation of Gly898 interferes with ergosterol binding, resulting in transcriptional activation of Upc2.

The shape complementarity of the binding pocket to the hydrocarbon rings of fungal sterols demonstrates the ligand specificity of the Upc2 LBD. Ergosterol and DHE have a double bond at C7–C8, while cholesterol has a single bond at the same position (Fig. 3a). The side chains of conserved Met902 and Leu906 directly contact the C7 atom of ergosterol (Fig. 3b). The cholesterol modeling in the pocket suggests that the H and C atoms at the C7 position make a steric clash with Met902, which explains the inability to bind cholesterol (Fig. 3c). To confirm this observation, we performed a DHE competition assay using 7-dehydrocholesterol (7-DHC) (Fig. 3d). Ergosterol competed with DHE for Upc2 binding, while cholesterol failed to replace DHE. However, 7-DHC bound well to Upc2, indicating the double bond at the C7 position is critical for the recognition of sterol ligands.

Conformational change upon sterol binding. The conformational change induced by sterol binding is the key process for transcriptional activation and nuclear transport of Upc2. Therefore, we compared the structures of the ergosterol-bound *Cg*Upc2/*Lt*Upc2 LBDs with apo *Sc*Upc2 LBD[11] (Protein Data Bank (PDB) ID 4N9N) (Fig. 4a). The α12 and CT are flexible in apo-form owing to the multiple glycine residues at their N termini. The reported structure of the apo ScUpc2 LBD lacking α12 and CT did not show a sterol-binding cavity[11]. The ligand binding generates conformational rearrangements in the C-terminal half of the LBD, creating a sterol-binding pocket (Fig. 4b). The cavity is formed by the expansion of the crevice between α6/7 and α11. The α11–α12 loop and α12, which were disordered in the ligand-free state, form the lid and cavity wall in the sterol-bound form.

We determined the structure of a *Sc*Upc2 LBD (residues 602–897) with a completely open conformation in fusion with T4 lysozyme at 3.5 Å resolution (Fig. 4c). We could not assign the residues in the α7 – α8 loop. However, the residues for other regions were

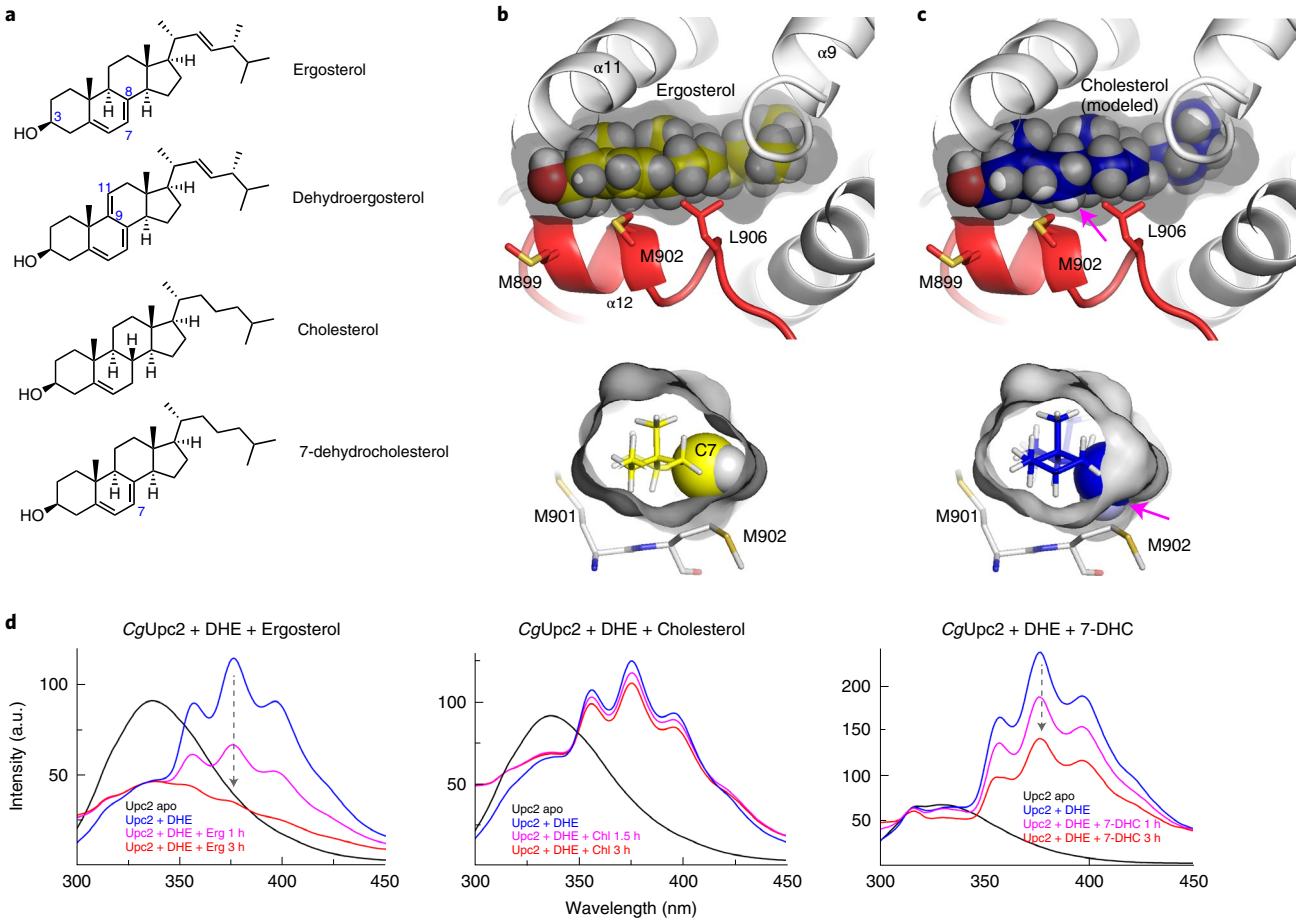

Fig. 3 | Ligand selectivity of the Upc2 LBD. a, Structures of sterol molecules used in this study. **b**, Ergosterol-binding pocket of *Cg*Upc2. The C7 atom and its hydrogen atom are shown in a sphere model. **c**, The cholesterol molecule was modeled into the pocket by replacing the bound ergosterol with cholesterol. The heterocyclic ring of cholesterol makes steric clashes with the binding pocket. The steric clash between the wall of the binding pocket and the modeled cholesterol was indicated by a magenta arrow. **d**, Sterol-binding assay of the *Cg*Upc2 LBD constructs. The competitive binding activities of non-fluorescent ergosterol, cholesterol, and 7-DHC were monitored against the DHE pre-bound to the Upc2 LBD at several time intervals. The dotted arrows indicate the time-lapse changes of fluorescence spectra. The spectral measurements were repeated two times, and one representative data was shown for each construct.

traceable in the electron density maps (Extended Data Fig. 2). The N-terminal half of the *Sc*Upc2 LBD has a similar conformation to the ergosterol-bound *Cg*Upc2. However, the C-terminal half of the LBD showed a completely open pocket (Fig. 4d). The sterol-binding pocket is open owing to the disorder of the α11–α12 loop and α12, exposing hydrophobic residues of the pocket (Fig. 4e). The helices α10 and α11 from a symmetry-related molecule cover the exposed pocket by lattice interaction (Fig. 4c). This open conformation of the apo *Sc*Upc2 LBD seems to represent an intermediate structure during ligand uptake and release. The structural analysis suggested that the Upc2 LBD has intrinsic conformational flexibility, which is essential for ligand-dependent conformational switching.

To examine the ligand-dependent flexibility of α12, we constructed an insertion mutant of a thrombin cleavage site at the α11–α12 loop (Fig. 2a and Extended Data Fig. 1b). The mutant displayed DHE-binding properties as observed for the wild type (Extended Data Fig. 4d). The stabilization of α12 by ligand binding made the α11–α12 loop less susceptible to thrombin cleavage. The α12–CT in the apo-form was efficiently cleaved off by thrombin. Ergosterol or 7-DHC binding substantially lowered the cleavage of α12–CT, while cholesterol treatment did not inhibit the cleavage (Fig. 4f). This result indicates the flexible α12 in the apo-form is stabilized by forming a cavity wall upon ligand binding. In apo-form, α12 is released from the LBD core and is exposed to the solvent. Helix α12 has amphipathic surfaces containing clusters of hydrophobic and hydrophilic residues (Fig. 4g). The hydrophobic patch of the exposed α12 is expected to interact with the hydrophobic residues of the CT by forming a hairpin conformation in the ligand-free state (Fig. 4g). In conclusion, the helix α12 is the key element for the conformational change and ligand recognition.

Importin α recognizes the Upc2 NLS for nuclear transport. To investigate the NLS recognition by importin α for the nuclear transport of Upc2, we determined the structures of *C. glabrata* importin α (*Cg*Impα) armadillo (ARM) domain in apo-form and in complex with the *Cg*Upc2 NLS (Supplementary Table 1). The Upc2 NLS was fused to the C terminus of the *Cg*Impα ARM domain to facilitate the crystallization of the complex. In the crystal lattice, the Upc2 NLS sequence from the tail of a neighboring molecule interacted with the concave groove of Impα in a head-to-tail fashion (Extended Data Fig. 5a). The entire chain of the Upc2 NLS was visible in the electron density maps suggesting stable interaction over the NLS sequence (Extended Data Fig. 2). The NLS binding induces a slight conformational change of N- and C-terminal ARM repeats towards the center to clamp the Upc2 NLS (Extended Data Fig. 5b). The Impα–Upc2 NLS interaction has a binding interface area of 472 Å^2

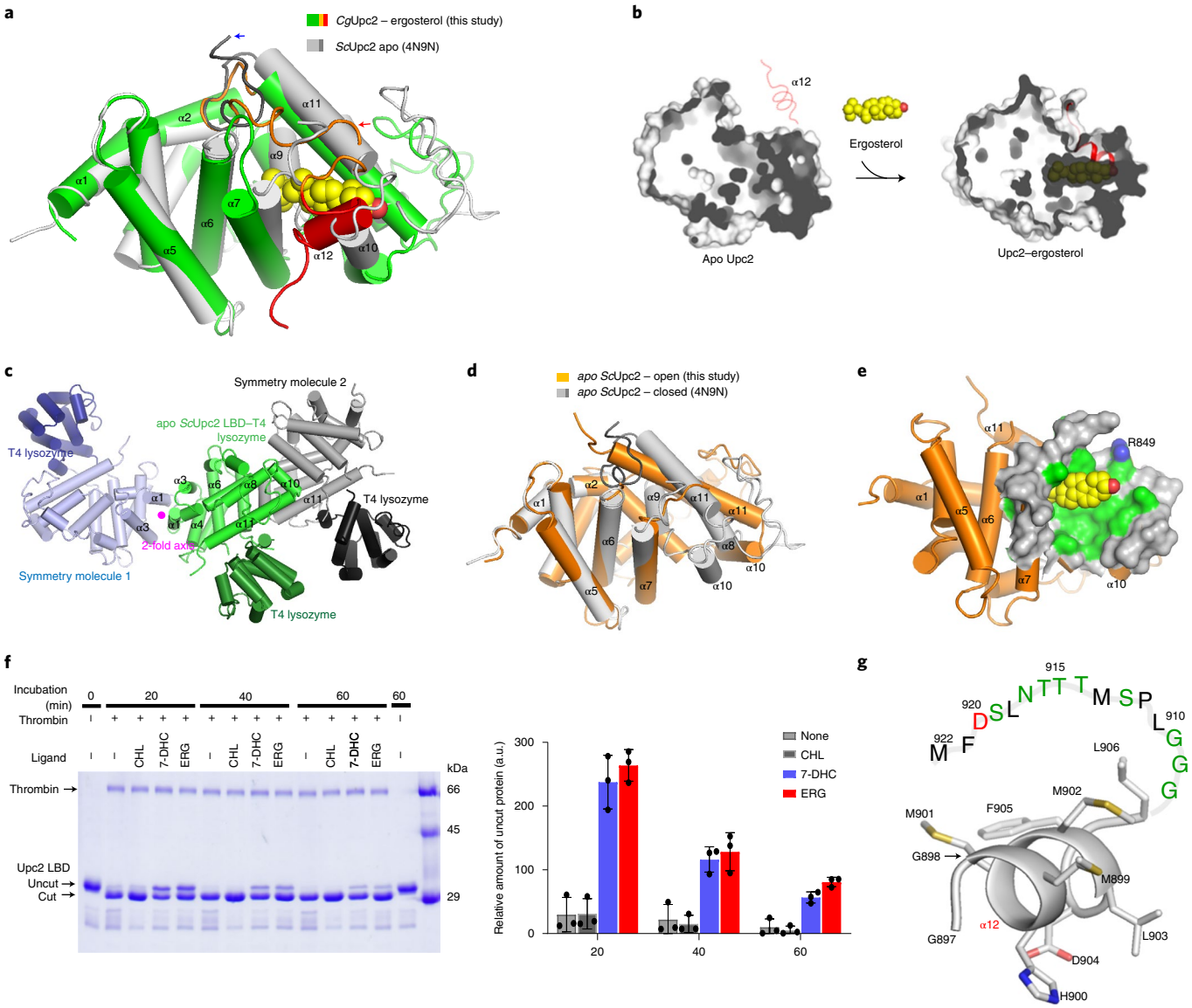

Fig. 4 | Conformational change of the Upc2 LBD upon sterol binding. a, Structural comparison of the ergosterol-bound *Cg*Upc2 LBD and apo *Sc*Upc2 LBD. The helix α12 of *Cg*Upc2 was colored in red. The blue and red arrows indicate the equivalent residues in the α11–α12 loops, Gln878 of *Sc*Upc2 and Arg888 of *Cg*Upc2, respectively, which shows conformational changes in the C-terminal region. **b**, Generation of the ligand-binding pocket upon ergosterol binding. The surface representations of *Sc*Upc2 LBD and *Cg*Upc2 LBD bound to ergosterol were shown. The helix α12 is indicated by red dotted lines and red ribbons for *Sc*Upc2 and *Cg*Upc2, respectively. **c**, The overall structure of apo *Sc*Upc2 LBD–T4 lysozyme fusion determined in this study. Two symmetry-related molecules contacting with the molecule in the asymmetric unit were shown in gray and blue. **d**, Structural comparison of the open and closed forms of the apo *Sc*Upc2 LBDs. The structures were aligned using the N-terminal half of the LBDs (α1–α6). **e**, Structure of the apo *Sc*Upc2 LBDs in an open conformation. The exposed sterol-binding pocket is shown in surface representation. The hydrophobic residues in the pocket are colored in green. The nitrogen atoms of Arg849 that make hydrogen bonds with the 3-hydroxyl group of ergosterol in closed conformation are shown in blue. The ergosterol from the *Cg*Upc2 LBD structure was shown to indicate the sterol-binding site in the open form. **f**, The conformation stabilization of helix α12 upon ligand binding. Ergosterol (ERG) and 7-DHC treatment reduced the proteolytic degradation of recombinant proteins, while cholesterol (CHL) treatment did not reduce the thrombin cleavage compared to the non-ligand control. The gel image is representative of three independent experiments. The bar graphs converted from the gel images are the averages of the three experiments with standard deviations. The individual data points for three-repeating experiments were overlaid in dots for each bar graph. **g**, The amphipathic helix α12 and the CT. The sixteen CT residues that were disordered in the crystal structures are shown in capital letters.

involving the surface of the ARM repeats 2–8 (Extended Data Fig. 5c,d). The interface is formed mainly by electrostatic interaction involving six hydrogen bonds, five salt bridges, and three cation-π interactions (Extended Data Fig. 6a,b). The two NLS-binding pockets on the concave surface of Impα are known as 'major' and 'minor' binding sites[26]. The major and minor binding sites contact the two basic clusters of [28]KR[29] and [41]HKKSK[45] of the Upc2 NLS, respectively. In addition, the residues [33]TS[34] and [38]R make hydrophilic interactions with the ARM 5 and 6. Structural comparison of the Impα–NLS complexes suggested that Upc2 displays a conserved NLS-binding mode in the major and minor binding sites with other NLS sequences (Extended Data Fig. 6c). The Upc2 NLS shows more variation in the backbone conformation between the two binding motifs than other NLS structures.

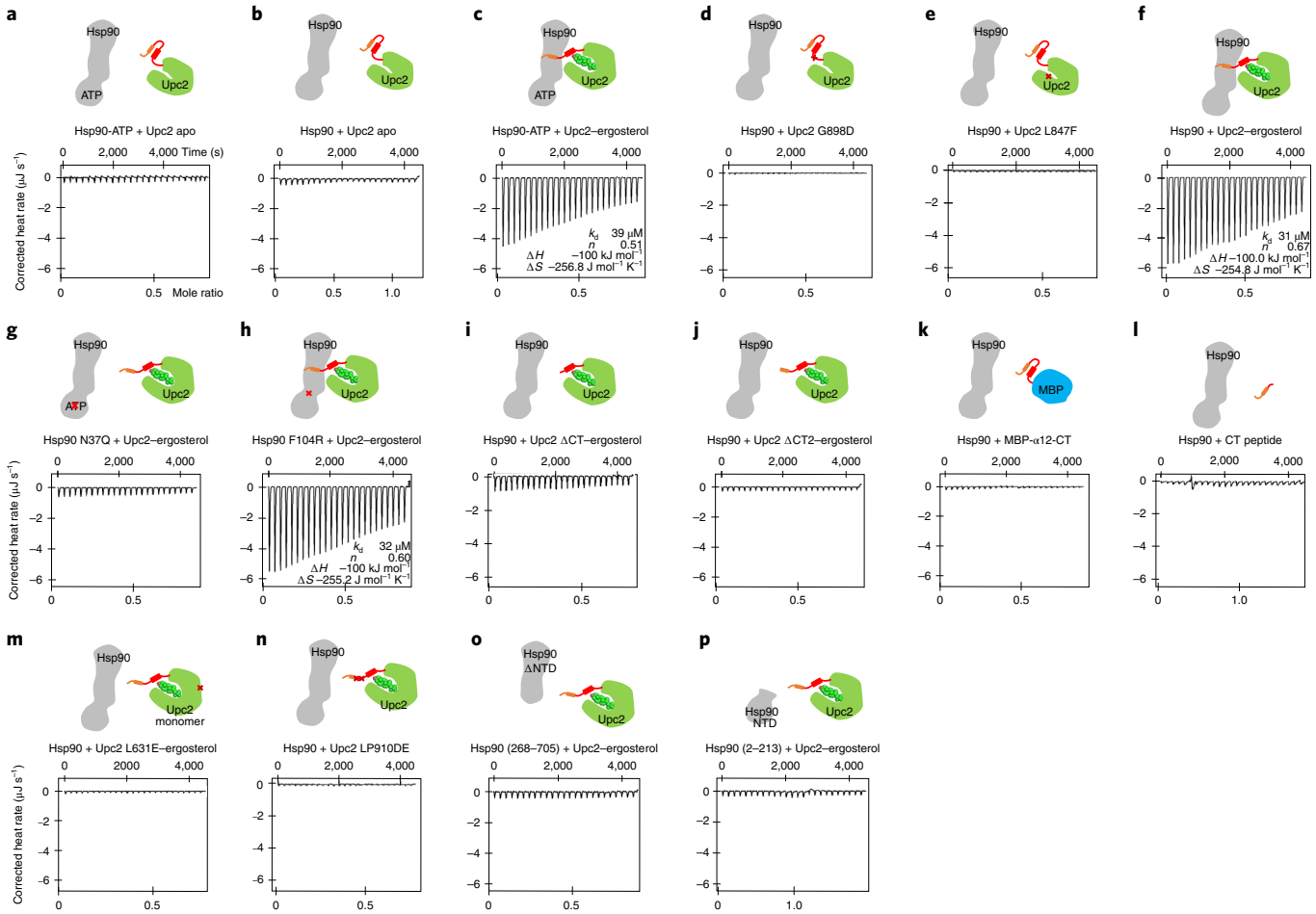

Fig. 5 | Sterol-dependent interaction of Hsp90 and Upc2 LBD. a–m, The ligand-dependent association of the *Cg*Upc2 LBD and *Cg*Hsp90 was examined by ITC. Recombinant *Cg*Hsp90 was loaded in the cell, and the various Upc2 LBD constructs in apo or ergosterol-bound forms were loaded in the syringe. *Cg*Hsp90 and *Cg*Upc2 are constitutive dimers in solution. To simplify the cartoon illustration of the experimental setup, the dimeric Upc2 and Hsp90 are shown as monomers. The actual monomeric *Cg*Upc2 LBD (L631E mutant) is indicated with a black 'monomer' label. The ITC experiments were repeated two times, yielding consistent results (Supplementary Fig. 3), and one representative titration curve was shown for each construct.

We measured the affinity of the Impα–Upc2 NLS interaction by isothermal titration calorimetry (ITC) (Extended Data Fig. 6d). The Upc2 NLS peptide (residues 26–46) or the maltose-binding protein (MBP) in fusion with the NLS (residues 16–48) showed affinities to Impα with K_d values of 1.3 and 1.2 μM, respectively. The strong binding correlates with the extensive molecular interaction observed in the structure of the Impα–NLS complex. The N200R mutation in the major binding site decreased the affinity to 9.3 μM, and the N200R/N368R mutation in both major and minor binding sites abolished the interaction. The mutations KR28–29DY and KK42–43DD in the Upc2 NLS decreased the affinity to the K_d value of 3.6 μM. In conclusion, these observations confirm that Upc2 has a canonical NLS–Impα interaction involving extensive contacts spanning the entire concave surface of Impα.

Upc2 associates with Hsp90 in a ligand-dependent manner. Even with the canonical NLS, the ergosterol-bound Upc2 is retained in the cytosol, suggesting the presence of a regulatory mechanism for the intracellular translocation. We hypothesized that the ligand-dependent association of Upc2 to the cytoplasmic Hsp90 is a key factor for cytosolic retention. We purified various recombinant *Cg*Hsp90 and *Cg*Upc2 LBD constructs (Supplementary Fig. 1) and examined the ergosterol-dependent protein interaction by ITC. The apo *Cg*Upc2 LBD did not interact with *Cg*Hsp90 whether ATP was provided or not (Fig. 5a,b). By contrast, the ergosterol-loaded *Cg*Upc2 LBD bound to *Cg*Hsp90 with the K_d value of 36 μM in the presence of 0.2 mM ATP (Fig. 5c). G898D and L847F mutants of *Cg*Upc2 in ligand-free forms did not interact with *Cg*Hsp90 (Fig. 5d,e). Without the ATP supplement to the purified *Cg*Hsp90, the ergosterol–Upc2 LBD interacted with the Hsp90 with a K_d value of 31 μM (Fig. 5f), suggesting the addition of ATP to Hsp90 is not essential for Upc2 binding. However, the N37Q mutation in the ATP-binding pocket, which inactivates Hsp90, abolished the interaction with Upc2 (Fig. 5g). By contrast, the F104R mutation outside the ATP-binding pocket of Hsp90 did not interfere with the Upc2 interaction (Fig. 5h). ATP binding to Hsp90 was known to change the conformational state of Hsp90, but ATP was not essential for client-protein binding to the M-domain[21,27]. Our data suggest that Hsp90–Upc2 interaction is sterol dependent and that functional Hsp90 is essential for the interaction. Since ergosterol is buried in the binding pocket, Hsp90 binding should be dependent on the conformation of the C-terminal half of the LBD. To identify the Hsp90-binding site in the Upc2 LBD, we examined the interaction using the C-terminal truncation constructs (ΔCT and ΔCT2) of *Cg*Upc2 LBD. The CT was disordered in the structures of the ergosterol-bound Upc2 LBDs. The ΔCT and ΔCT2 mutants lacking the C-terminal 13 and 2 residues, respectively, showed similar DHE-binding properties to wild type (Extended Data Fig. 4f,g). However, the CT deletion mutants did

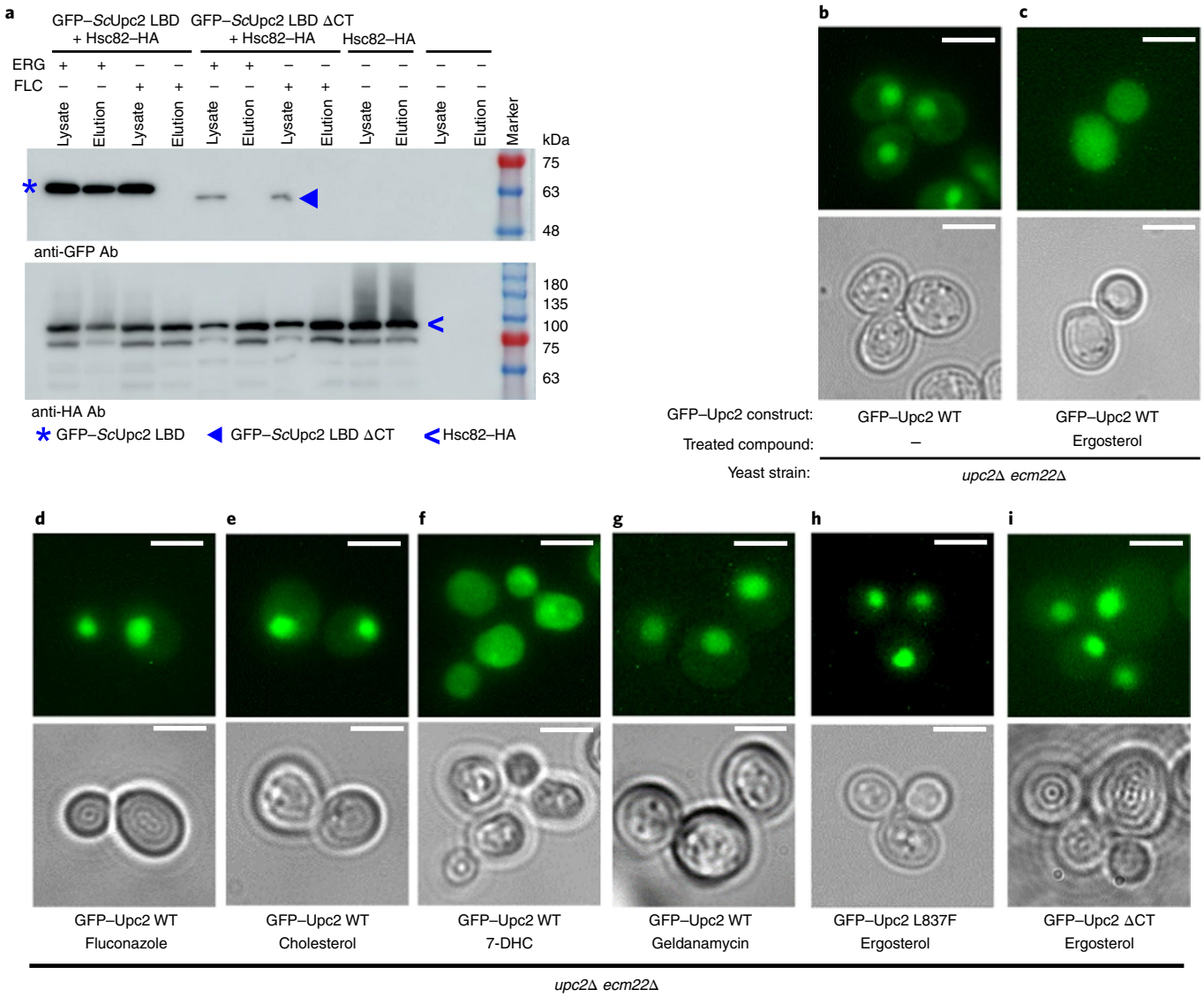

Fig. 6 | Sterol-dependent Hsp90 interaction and the localization of Upc2. a, Co-immunoprecipitation of the HA-tagged *Sc*Hsc82 and GFP-*Sc*Upc2 LBD and Western Blot analysis. Lanes 1–4 are the yeast *hsc82Δ* cells co-transformed with the plasmids encoding GFP-*Sc*Upc2 LBD and *Sc*Hsc82-HA. Lanes 5–8 are the cells co-transformed with the plasmids encoding *Sc*Upc2 LBD ΔCT and *Sc*Hsc82-HA. Lanes 9 and 10 are the cells transformed with only *Sc*Hsc82-HA plasmid. Lanes 11 and 12 are the non-transformed cells used as a negative control. The identical gel was used for the detection of *Sc*Upc2 LBD and *Sc*Hsc82 by anti-GFP and anti-HA antibodies. The experiments were repeated two times and the representative western blot images are shown. **b–i**, Yeast cell imaging of GFP-*Sc*Upc2 for Hsp90-dependent nuclear translocation. The *upc2Δ ecm22Δ* cells expressing GFP-*Sc*Upc2 constructs were grown with 4 μg ml^{-1} of fluconazole or 5 mM of sterols (ergosterol, cholesterol, and 7-DHC) for 12 h before visualization by fluorescence microscopy. The Hsp90-specific inhibitor, geldanamycin was treated with 2 μM to inactivate the Hsp90 in the presence of ergosterol. The microscopic imaging of the yeast cells was repeated two times with consistent results. More than 300 cells were examined, and the cell images representing more than 80% of the cell population were shown in the panels. The top panels show the localization of GFP-ScUpc2. The nuclear localization of Upc2 appears as a bright green sphere inside the cell. Scale bars, 3 μm.

not bind Hsp90 (Fig. 5i,j), indicating that the CT region is involved in Hsp90 association in a ligand-dependent manner. However, the isolated CT peptides (906–922), either in a free form or in an MBP fusion, did not bind Hsp90 (Fig. 5k,l). The L631E mutation in the dimer interface retained the sterol-binding activity but resulted in the monomerization of the Upc2 LBD (Extended Data Fig. 4e and Supplementary Fig. 2). The ergosterol-loaded L631E mutant did not interact with Hsp90 (Fig. 5m), suggesting that the dimeric configuration of Upc2 is critical for Hsp90 association.

These data imply that the ligand-dependent conformation of the CT is essential for Hsp90 association. The flexible CT of the ergosterol-bound Upc2 is exposed to the solvent, allowing Hsp90 interaction. Upon ligand dissociation, the helix α12 is released from the LBD core to the solvent exposing the hydrophobic face of the amphipathic helix (Fig. 4g). The hydrophobic patch of the released α12 seems to interact with the hydrophobic residues of the CT, masking the key residues in the CT, and subsequently inhibiting the interaction with Hsp90.

The recent structural analyses of the human Hsp90–GR–co-chaperone complex revealed that the Hsp90 dimer associates with the partially unfolded N-terminal extension of the GR LBD[28,29]. The sequence alignment of the *Cg*Upc2 CT and the N-terminal upstream

of the GR LBD suggests the Hsp90-binding motif might be present in Upc2 (Extended Data Fig. 7a). The extended loop residues ^{525}LPQLT^{529} of GR interacted with Met614 and Leu619 in the central lumen of human Hsp90 (ref. [28]) (Extended Data Fig. 7b,c). The Upc2 LBD contains ^{910}LPSMT^{914} in the CT, which is similar to the Hsp90-binding motif of the GR, implying conservation of client-binding modes. We examined the interaction of various *Cg*Hsp90 and Upc2 LBD mutants to identify the binding mode. The LP910-911DE mutation of the potential Hsp90-binding motif in *Cg*Upc2 abolished the interaction with Hsp90 (Fig. 5n). The isolated domains of Hsp90 (N- and M/C-domain) did not bind the Upc2 LBD–ergosterol, suggesting intact Hsp90 is required for Upc2 binding (Fig. 5o,p). L594T or M589E mutation in the central lumen of *Cg*Hsp90 abolished the Upc2 LBD binding (Extended Data Fig. 8a). By contrast, F579E mutation located far from the client-binding site of *Cg*Hsp90 did not interfere with *Cg*Upc2 binding (Extended Data Fig. 8a). This data suggests that *Cg*Hsp90 utilizes the equivalent binding site for Upc2 association as observed for the human Hsp90–GR interaction.

S. cerevisiae contains two cytoplasmic isoforms, Hsp82 and Hsc82 (ref. [30]). To examine the conservation of the Upc2–Hsp90 interaction in *S. cerevisiae*, we analyzed the binding of the *Sc*Upc2 LBD to *Sc*Hsc82/*Sc*Hsp82 (Extended Data Fig. 8b). *Sc*Upc2 LBD interacted with *Sc*Hsp90 isoforms in a ligand-dependent manner. However, M589E mutation in *Sc*Hsc82 abolished the interaction with *Sc*Upc2. This observation indicates that the Upc2–Hsp90 interaction is conserved in *S. cerevisiae* and *C. glabrata*. In conclusion, the ergosterol-bound Upc2 associates with Hsp90 using the exposed CT, which retains the inactive Upc2 in the cytosol (Extended Data Fig. 8c). *Cg*Upc2 associates weakly with Hsp90 compared to the interaction with the importin α, suggesting that Hsp90–Upc2 interaction is readily reversible by conformation changes upon ligand binding and release.

Cytosolic retention of Upc2 is mediated by Hsp90. To confirm the Hsp90–Upc2 interaction, we examined the interaction of GFP–*Sc*Upc2 LBD and HA (Hemagglutinin)-tagged *Sc*Hsc82 expressed in the *hsc82Δ* yeast cells by co-immunoprecipitation. We captured the *Sc*Hsc82 by anti-HA resin from the yeast cell lysate and examined the co-pulldown of the GFP–*Sc*Upc2 LBD. *Sc*Upc2 LBD was co-precipitated with *Sc*Hsc82 in an ergosterol-dependent manner (Fig. 6a). The GFP–ScUpc2 LBD co-precipitated with *Sc*Hsc82 when ergosterol was treated, while the interaction was lost upon fluconazole treatment. However, the ΔCT mutant did not co-precipitate with *Sc*Hsc82 in the same experimental conditions.

To investigate the Hsp90-mediated cytosolic retention of *Sc*Upc2 in yeast cells, we monitored the intracellular localization of the GFP–*Sc*Upc2 constructs in various conditions. Without ergosterol supplement, GFP–*Sc*Upc2 was localized both in the nucleus and in the cytosol (Fig. 6b). However, the addition of ergosterol to the yeast culture shifted the localization of *Sc*Upc2 to the cytosol as previously reported[11] (Fig. 6c). Fluconazole treatment shifted the localization of *Sc*Upc2 entirely to the nucleus (Fig. 6d). Cholesterol treatment showed nuclear localization of GFP–ScUpc2 (Fig. 6e). However, 7-DHC treatment changed the localization of Upc2 to the cytosol (Fig. 6f), which is consistent with the ligand-binding data and structural analysis of the Upc2 LBDs.

To test the regulatory role of Hsp90 in *Sc*Upc2 localization, we examine the localization in the presence of a specific Hsp90 inhibitor, geldanamycin. It inhibits the ATPase activity of fungal and mammalian Hsp90 by tightly binding to the nucleotide-binding domain[31]. Inactivation of Hsc82 and Hsp82 by geldanamycin shifted the localization of *Sc*Upc2 to the nucleus regardless of ergosterol treatment (Fig. 6g), suggesting that functional Hsp90 is critical for the cytosolic retention of *Sc*Upc2. The L837F mutant lacking ligand-binding property showed nuclear localization, confirming that the ergosterol-loaded *Sc*Upc2 associates with Hsp90 (Fig. 6h). The ΔCT mutant of *Sc*Upc2 (residues 1–909) did not interact with Hsp90 in ITC experiments. Consistently, the GFP–ScUpc2 ΔCT showed nuclear localization in the presence of ergosterol (Fig. 6i), confirming that the CT region is essential for Hsp90 association. Since the double knockout of *HSC82* and *HSP82* is lethal in *S. cerevisiae*[30], we examined the localization of various *Sc*Upc2 constructs in single knockout cells of *HSC82* or *HSP82*. If ergosterol was supplemented in the cell culture, *Sc*Upc2 was cytosolic in the strain containing both Hsp82 and Hsc82 (Extended Data Fig. 9a). However, single knockout cells lacking either Hsp82 or Hsc82 showed nuclear localization of Upc2 (Extended Data Fig. 9b,c). Both Hsp90 isoforms are required to retain *Sc*Upc2 in the cytosol, suggesting that a sufficient number of Hsp90 is required for the cytosolic retention of *Sc*Upc2. The deletion of NLS-DBD resulted in cytosolic distribution, while the deletion of CT showed nuclear localization as expected (Extended Data Fig. 9d,e). In conclusion, Hsp90 and importin α are the key proteins assisting the cellular localization of Upc2.

Regulation of transcriptional activity and azole resistance. We examined the transcription activity, cellular sterol level, and azole susceptibility of the yeast *upc2Δ ecm22Δ* cells transformed with various *Sc*Upc2 constructs (Extended Data Fig. 10a–c). Since Upc2 activates the expression of ergosterol biosynthetic genes, the sterol levels and azole resistance of the yeast cells are expected to correlate with the transcriptional activities of Upc2. In the *upc2Δ ecm22Δ* double knockout cells lacking *Sc*Upc2, sterol levels were weakly detectable, and the addition of 4 μg ml^{-1} fluconazole severely inhibited the cell growth. *Sc*Upc2 G888D (corresponding to *Cg*Upc2 G898D) showed constitutive transcriptional activity as previously reported[11]. The transcription activity of L855F mutant was similar to the wild type, which correlates with the sterol-binding properties of L855F and the wild type. L837F mutation of *Sc*Upc2 (L847F in *Cg*Upc2) interfered with sterol binding and Hsp90 interaction (Fig. 5e and Extended Data Fig. 4b). However, the L837F mutant was almost transcriptionally inactive compared to the wild type, suggesting the bulky mutation in the binding cavity might have interfered with the conformation required for transcriptional activation. Consistently, the L837F mutant had a lower sterol level and was more susceptible to fluconazole than the wild type (Extended Data Fig. 10b,c). The transcriptional activities and sterol levels of the mutants (L837F, L855F, and ΔCT) were lower than the wild type, while G888D mutant showed substantially higher transcriptional activity and sterol level, suggesting that the C-terminal Gly-rich loop is involved in the transcriptional regulation as well as cellular translocation of Upc2. These data explain why the constitutively active mutations are clustered in the Gly-rich loop and not observed in the hydrophobic cavity in azole-resistant mutants. In conclusion, these data suggest ergosterol-dependent regulation of transcription and Hsp90-mediated intracellular translocation of Upc2.

Discussion

Many Zinc cluster transcription factors in fungi recognize small-molecule ligands and regulate transcription governing biological functions such as metabolism and response to environmental cues[32]. In this study, we elucidated the ligand specificity and the mechanism of transcription regulation and azole resistance by Upc2. Since most of the cellular ergosterol is present in the plasma membrane, sensing the ergosterol level in the cytosol and regulating the transcription of related genes in the nucleus are crucial for fungal cells. The living environment of the pathogenic *Candida* species is the human tissues, which contain abundant sources of cholesterol. Therefore, the specificity of Upc2 toward ergosterol is crucial to avoid the interference of cholesterol on the regulatory pathway of ergosterol homeostasis. Eukaryotes contain several superfamilies of sterol-transfer proteins that bind many different types of sterols[33].

By contrast, Upc2 specifically recognizes ergosterol and DHE using a shape-complementary pocket with the 3-hydroxyl group located at the tunnel entrance. Two Upc2 homologs in *S. cerevisiae*, *Sc*Upc2 and *Sc*Ecm22, have high sequence conservation in the DBDs and LBDs, suggesting preservation of the target genes and mechanism of transcriptional regulation, correlating with their overlapping functions[8]. Both proteins are involved in sterol-mediated regulation of *ERG2* and *ERG3* by binding to the same 7-bp regulatory sequence[8]. However, only Upc2A out of two Upc2 homologs in *C. glabrata* was shown to influence azole susceptibility[10]. Upc2B has sequence variations in the DBD compared to Upc2A, implying different specificities on the target gene promoters despite the identical mode of transcriptional regulation by ergosterol.

Metazoan nuclear receptors serve as direct signal sensors by binding and responding to small lipophilic molecules. Hsp90 forms stable complexes with steroid receptors in mammals and promotes receptor activation by maintaining a high-affinity ligand-binding conformation[21,34]. Even though there is no sequence similarity of Upc2 to the nuclear receptors, our data reveals mechanistic similarities of fungal Upc2 orthologs to the steroid receptors in terms of transcription regulation and Hsp90-mediated translocation. Hsp90–client interaction is often assisted by diverse co-chaperones which are specific to the client proteins[27]. Co-chaperones stabilize the Hsp90 complex by bridging Hsp90 and client proteins by direct interaction[27]. Therefore, the Upc2 co-chaperones currently unknown might assist the stable association of Hsp90 and Upc2 by forming a high molecular weight complex as observed for the Hsp90–Hap1 interaction[35].

In conclusion, we have elucidated the molecular mechanism of Upc2 translocation mediated by importin α and Hsp90. This work reveals the structural determinants for sterol recognition, transcriptional regulation, and acquisition of azole resistance by Upc2. This structural study provides a new antifungal target with a well-defined ligand-binding pocket for the development of co-therapeutics that might improve standard azole therapies. Small-molecule agonists might lock Upc2 in an inactive conformation or interfere with co-activator binding, thereby preventing activation of sterol biosynthetic genes and resulting in sensitization to azole drugs against *Candida* species.

Online content

Any methods, additional references, Nature Research reporting summaries, source data, extended data, supplementary information, acknowledgements, peer review information; details of author contributions and competing interests; and statements of data and code availability are available at https://doi.org/10.1038/s41589-022-01117-0.

Received: 20 October 2021; Accepted: 20 July 2022;
Published online: 13 October 2022

References

1. Maguire, S. L. et al. Zinc finger transcription factors displaced SREBP proteins as the major Sterol regulators during Saccharomycotina evolution. *PLoS Genet.* **10**, e1004076 (2014).
2. Perfect, J. R. The antifungal pipeline: a reality check. *Nat. Rev. Drug Disco.* **16**, 603–616 (2017).
3. Whaley, S. G. et al. Azole antifungal resistance in *Candida albicans* and emerging non-albicans *Candida* species. *Front Microbiol* **7**, 2173 (2016).
4. Anderson, J. B. Evolution of antifungal-drug resistance: mechanisms and pathogen fitness. *Nat. Rev. Microbiol.* **3**, 547–556 (2005).
5. Cowen, L. E., Sanglard, D., Howard, S. J., Rogers, P. D. & Perlin, D. S. Mechanisms of antifungal drug resistance. *Cold Spring Harb. Perspect. Med* **5**, a019752 (2014).
6. Rogers, P. D. & Barker, K. S. Genome-wide expression profile analysis reveals coordinately regulated genes associated with stepwise acquisition of azole resistance in *Candida albicans* clinical isolates. *Antimicrob. Agents Chemother.* **47**, 1220–1227 (2003).
7. MacPherson, S. et al. *Candida albicans* zinc cluster protein Upc2p confers resistance to antifungal drugs and is an activator of ergosterol biosynthetic genes. *Antimicrob. Agents Chemother.* **49**, 1745–1752 (2005).
8. Vik, A. & Rine, J. Upc2p and Ecm22p, dual regulators of sterol biosynthesis in *Saccharomyces cerevisiae*. *Mol. Cell. Biol.* **21**, 6395–6405 (2001).
9. Davies, B. S., Wang, H. S. & Rine, J. Dual activators of the sterol biosynthetic pathway of *Saccharomyces cerevisiae*: similar activation/regulatory domains but different response mechanisms. *Mol. Cell. Biol.* **25**, 7375–7385 (2005).
10. Whaley, S. G. et al. *UPC2A* is required for high-level azole antifungal resistance in *Candida glabrata*. *Antimicrob. Agents Chemother.* **58**, 4543–4554 (2014).
11. Yang, H. et al. Structural mechanism of ergosterol regulation by fungal sterol transcription factor Upc2. *Nat. Commun.* **6**, 6129 (2015).
12. Moye-Rowley, W. S. Linkage between genes involved in azole resistance and ergosterol biosynthesis. *PLoS Pathog.* **16**, e1008819 (2020).
13. Jorda, T. & Puig, S. Regulation of ergosterol biosynthesis in *Saccharomyces cerevisiae*. *Genes* **11**, 795 (2020).
14. Vasicek, E. M., Berkow, E. L., Flowers, S. A., Barker, K. S. & Rogers, P. D. *UPC2* is universally essential for azole antifungal resistance in *Candida albicans*. *Eukaryot. Cell* **13**, 933–946 (2014).
15. Dunkel, N. et al. A gain-of-function mutation in the transcription factor Upc2p causes upregulation of ergosterol biosynthesis genes and increased fluconazole resistance in a clinical *Candida albicans* isolate. *Eukaryot. Cell* **7**, 1180–1190 (2008).
16. Heilmann, C. J., Schneider, S., Barker, K. S., Rogers, P. D. & Morschhauser, J. An A643T mutation in the transcription factor Upc2p causes constitutive *ERG11* upregulation and increased fluconazole resistance in *Candida albicans*. *Antimicrob. Agents Chemother.* **54**, 353–359 (2010).
17. Hoot, S. J., Smith, A. R., Brown, R. P. & White, T. C. An A643V amino acid substitution in Upc2p contributes to azole resistance in well-characterized clinical isolates of *Candida albicans*. *Antimicrob. Agents Chemother.* **55**, 940–942 (2011).
18. Flowers, S. A. et al. Gain-of-function mutations in *UPC2* are a frequent cause of *ERG11* upregulation in azole-resistant clinical isolates of *Candida albicans*. *Eukaryot. Cell* **11**, 1289–1299 (2012).
19. Backe, S. J., Sager, R. A., Woodford, M. R., Makedon, A. M. & Mollapour, M. Post-translational modifications of Hsp90 and translating the chaperone code. *J. Biol. Chem.* **295**, 11099–11117 (2020).
20. Leach, M. D., Klipp, E., Cowen, L. E. & Brown, A. J. Fungal Hsp90: a biological transistor that tunes cellular outputs to thermal inputs. *Nat. Rev. Microbiol.* **10**, 693–704 (2012).
21. Pearl, L. H. & Prodromou, C. Structure and mechanism of the Hsp90 molecular chaperone machinery. *Annu. Rev. Biochem.* **75**, 271–294 (2006).
22. Murphy, P. J. Regulation of glucocorticoid receptor steroid binding and trafficking by the hsp90/hsp70-based chaperone machinery: implications for clinical intervention. *Leukemia* **19**, 710–712 (2005).
23. Diezmann, S., Michaut, M., Shapiro, R. S., Bader, G. D. & Cowen, L. E. Mapping the Hsp90 genetic interaction network in *Candida albicans* reveals environmental contingency and rewired circuitry. *PLoS Genet.* **8**, e1002562 (2012).
24. Van Hauwenhuyse, F., Fiori, A. & Van Dijck, P. Ascorbic acid inhibition of *Candida albicans* Hsp90-mediated morphogenesis occurs via the transcriptional regulator Upc2. *Eukaryot. Cell* **13**, 1278–1289 (2014).
25. Le Fur, Y., Maume, G., Feuillat, M. & Maume, B. F. Characterization by gas chromatography/mass spectrometry of sterols in *Saccharomyces cerevisiae* during autolysis. *J. Agric. Food Chem.* **47**, 2860–2864 (1999).
26. Fontes, M. R., Teh, T., Jans, D., Brinkworth, R. I. & Kobe, B. Structural basis for the specificity of bipartite nuclear localization sequence binding by importin-α. *J. Biol. Chem.* **278**, 27981–27987 (2003).
27. Lorenz, O. R. et al. Modulation of the Hsp90 chaperone cycle by a stringent client protein. *Mol. Cell* **53**, 941–953 (2014).
28. Noddings, C. M., Wang, R. Y., Johnson, J. L. & Agard, D. A. Structure of Hsp90–p23–GR reveals the Hsp90 client-remodelling mechanism. *Nature* **601**, 465–469 (2022).
29. Wang, R. Y. et al. Structure of Hsp90–Hsp70–Hop–GR reveals the Hsp90 client-loading mechanism. *Nature* **601**, 460–464 (2022).
30. Borkovich, K. A., Farrelly, F. W., Finkelstein, D. B., Taulien, J. & Lindquist, S. hsp82 is an essential protein that is required in higher concentrations for growth of cells at higher temperatures. *Mol. Cell. Biol.* **9**, 3919–3930 (1989).
31. Nicola, A. M. et al. The stress responsive and morphologically regulated hsp90 gene from *Paracoccidioides brasiliensis* is essential to cell viability. *BMC Microbiol.* **8**, 158 (2008).
32. Naar, A. M. & Thakur, J. K. Nuclear receptor-like transcription factors in fungi. *Genes Dev.* **23**, 419–432 (2009).
33. Luo, J., Jiang, L. Y., Yang, H. & Song, B. L. Intracellular cholesterol transport by sterol transfer proteins at membrane contact sites. *Trends Biochem. Sci.* **44**, 273–292 (2019).
34. Pratt, W. B. & Toft, D. O. Regulation of signaling protein function and trafficking by the hsp90/hsp70-based chaperone machinery. *Exp. Biol. Med.* **228**, 111–133 (2003).

35. Lee, H. C., Hon, T. & Zhang, L. The molecular chaperone Hsp90 mediates heme activation of the yeast transcriptional activator Hap1. *J. Biol. Chem.* **277**, 7430–7437 (2002).

Methods

Cloning of Upc2, Importin α, and Hsp90. The genes for Upc2, Importin α, and Hsp90 were amplified by PCR using *S. cerevisiae*, *C. glabrata* and *L. thermotolerans* genomic DNA as templates. The DNA encoding the C-terminal ligand-binding domains (LBDs) of *Cg*Upc2 (UniProt ID Q6FX18) and *Lt*Upc2 (UniProt ID C5DKV6) were subcloned into the BamHI/XhoI site of a modified pHIS2 vector[36]. The Upc2 LBDs were tagged with the N-terminal hexahistidine followed by a thrombin protease cleavage site (LVPR/GS). To improve the crystallization properties by surface entropy reduction, the flexible loop (residues 588–600) of *Lt*Upc2 was truncated. The DNA encoding the ARM domain (residues 76–516) of *Cg*Impα (UniProt ID Q6FNI4) was subcloned into the BamHI/XhoI site of the modified pHIS2 vector. For the structural studies of the importin α–NLS complex, the chimeric protein of *Cg*Impα ARM domain–Upc2 NLS was made by fusing the NLS sequence (residues 24–47) to the C terminus of the ARM domain using a thrombin cleavage site (LVPR/GS) as a linker. The full-length constructs of *Sc*Hsp82 (UniProt ID P02829), *Sc*Hsc82 (UniProt ID P15108), and *Cg*Hsp90 (UniProt ID Q6FLU9) were cloned to the BamHI/XhoI site of the pHIS2 vector.

Protein expression and purification. *Escherichia coli* strain BL21(DE3) cells transformed with the plasmids encoding the Upc2 constructs were grown to an OD_{600} of 0.8 at 37 °C in LB medium. Cells were induced by adding isopropyl β-D-1-thiogalactopyranoside to a final concentration of 0.5 mM and were incubated for 12 h overnight at 20 °C before collection. The cells were resuspended in 2× phosphate-buffered saline (PBS) containing additional 20 mM imidazole (lysis buffer) and lysed by sonication. The supernatant containing the His-tagged Upc2 LBD was loaded to a Ni-NTA affinity column. The Ni-NTA column was washed with the lysis buffer. The target protein was eluted from the column using a buffer containing 100 mM Tris-HCl pH 8.0 (final), 300 mM imidazole. The eluate was concentrated to 10 mg ml^{-1} using Amicon Ultra-15 centrifugal filter. The His-tag was cleaved by 10 international units (IU) of thrombin protease (Reyon Pharmaceutical) per 10 mg of recombinant protein. The cleaved sample was subjected to size exclusion chromatography (SEC) on a HiLoad Superdex 200 column equilibrated with 20 mM Tris-HCl pH 8.0, 150 mM NaCl. The fractions containing the Upc2 LBDs were concentrated by the centrifugal filter to 10 mg ml^{-1} for crystallization. The ergosterol-loaded Upc2 LBDs were prepared by supplementing 2 mM of ergosterol to the cell culture, cell lysate, and the Ni-NTA affinity elutes. The importin α ARM domain and its Upc2 NLS fusion construct were expressed and purified using the same procedures described for the purification of the Upc2 LBD. The constructs for *Cg*Hsp90 and *Sc*Hsp90 chaperones were expressed and purified using the procedures for the Upc2 LBD.

Crystallographic analysis of Upc2 and importin α–NLS. Ergosterol solubilized in dimethyl sulfoxide (DMSO) was added to the Upc2 LBD samples with a final 2 mM concentration before SEC. Subsequent SEC removed DMSO from the protein sample, which was essential for crystallization of the ergosterol-loaded Upc2 LBD. Preliminary crystallization experiments were carried out at 22 °C in 96-well crystallization plates using customized crystallization screening solutions by dispensing 0.8 µl protein solution and 0.8 µl precipitant solution. The crystals of the *Cg*Upc2 LBD–ergosterol appeared in two weeks using a solution consisting of 0.1 M Na-Acetate pH 4.0, 10% PEG 4000, 0.1 M Na_3Citrate in the 96-well plates. The crystals of the *Lt*Upc2 LBD–ergosterol grown in a condition composed of 0.1 M Na-Acetate pH 4.0, 15% PEG 20000, 0.2 M $NaNO_3$. The crystallization condition was further optimized using the hanging-drop technique in 15-well screw-cap plates. A drop consisting of 1.5 µl protein solution was mixed with 1.5 µl precipitant solution and equilibrated against 1 ml reservoir solution. High-quality crystals with dimensions of 0.1 × 0.1 × 0.15 mm appeared in a week. Crystals of the Upc2 LBDs were cryoprotected in the reservoir solution supplemented with 15% glycerol and flash cooled by immersing in liquid nitrogen. Crystals were preserved in a cryogenic nitrogen gas stream during diffraction experiments. Native diffraction data for the Upc2 LBDs were collected at a fixed wavelength of 0.97934 Å using an ADSC Q270 CCD detector on the 7A beamline at Pohang Light Source (PLS), Pohang Accelerator Laboratory. All data were processed and scaled using HKL2000. The structures of *Cg*Upc2 and *Lt*Upc2 LBDs were determined by molecular replacement using the structure of apo *Sc*Upc2 LBD (PDB ID 4N9N) as a search model using the program Phaser. Four molecules of the Upc2 LBDs as two copies of dimers were present in the asymmetric unit of the crystals. The bound ergosterol molecules were clearly visible in the electron density maps. The models were built using the software Coot, and the final models were refined to R_{free} values of 25.2% and 28.1% for *Cg*Upc2 and *Lt*Upc2, respectively, using Phenix[37]. The structure figures were drawn using PyMOL (https://pymol.org).

The crystals of the importin α ARM domain and its Upc2 NLS fusion were grown in the buffer conditions composed of 0.1 M Tris-HCl pH 7.0, 30% PEG 8000, 0.4 M NaCl, and 0.1 M Tris-HCl pH 8.0, 30% PEG 400, respectively. The diffraction data for the apo importin α and the NLS fusion were collected at 2.3 and 2.5 Å resolution, respectively. The structures of *Cg*Impα were solved by molecular replacement using *Sc* importin α (PDB ID 4XGR) as a search model, and the structures were refined to R_{free} values of 26.9% and 26.2%, respectively.

Crystallographic studies of the apo *Sc*Upc2 LBD. The DNA encoding the *Sc*Upc2 LBD (residues 602–897) containing the helix α12 was cloned to the NdeI and XhoI sites of a pET28b vector. The variable α6–α7 loop (residues 715–725) was replaced by a T4 lysozyme (T4L) to improve the crystallization properties of the construct as previously described[11]. The plasmid containing the *Sc*Upc2 LBD–T4L was transformed to *E. coli* strain BL21(DE3). The protein was purified with a similar procedure used for the purification of the *Cg*Upc2 LBD. The crystal was grown in a condition composed of 0.1 M HEPES pH 7.0, 12.5% PEG 8000, 0.2 M sodium citrate. The diffraction data were collected to 3.5 Å resolution at a fixed wavelength of 0.97934 Å using an ADSC Q270 CCD detector on the 7A beamline at PLS and processed with HKL2000. The space group was $C222_1$ with one molecule in an asymmetric unit. The dimer of the *Sc*Upc2 LBD was formed by the 2-fold crystallographic symmetry axis. The structure was solved by molecular replacement using the structure of apo *Sc*Upc2 LBD (residues 598–878)–T4 lysozyme (PDB ID 4N9N). The N-terminal half of the T4 lysozyme was disordered and not included in the structure model. The *Sc*Upc2 LBD spanning the residues 605–870 were visible in the electron density maps owing to the disorder of the α11–α12 loop and helix α12. The sterol-binding pocket was completely open, exposing hydrophobic residues. The helices α10 and α11 from the symmetry-related molecule formed a crystal lattice interaction with the exposed sterol-binding pocket. The structure was refined to the final R_{work}/R_{free} values of 26.1 and 30.6%, respectively.

Thrombin cleavage assay of the α11–α12 loop. To examine the stabilization of helix α12 upon ligand binding, we monitored the thrombin cleave efficiency of the α11–α12 loop. The thrombin protease recognition sequence with two glycine linkers (GG-LVPR/GS-GG) was inserted between the residues 894 and 895 in the α11–α12 loop by mutagenesis. The unliganded Upc2 with an open conformation of α12 was expected to be more susceptible to thrombin cleavage than the ligand-bound form. The ligand-binding activity of the insertion mutant was confirmed by a DHE-binding assay. Cholesterol, ergosterol, and 7-DHC were treated with a final 2 mM to the purified proteins before SEC to avoid the contamination of the organic solvent used for solubilizing the sterol compounds. The 150 µl of 0.6 mg ml^{-1} purified Upc2 LBD loaded with sterol or in apo-form was mixed with 0.2 U of thrombin and incubated at room temperature with time intervals of 20, 40, and 60 min. The cleavage of incubated protein samples was analyzed by SDS-PAGE. The band intensities of the scanned gel image were quantified using ImageJ software.

Liposome preparation. DOPC was obtained from Avanti Polar Lipids. Ergosterol and DHE were obtained from Sigma-Aldrich. Lipids solubilized in chloroform or in ethanol were mixed at the desired molar ratio and incubated at 37 °C for 5 min. Subsequently, the solvent was evaporated by a nitrogen gas stream. The dried lipid pellet was resuspended in 50 mM HEPES, pH 7.2, and 120 mM potassium acetate by vortexing. The liposomes were prepared at a total lipid concentration of 1.3 mM. The hydrated lipid mixture was frozen and thawed five times using a water bath and cooled ethanol at −70 °C. The lipid mixture was extruded ten times through a polycarbonate filter with a pore size of 0.1 µm. Liposomes were stored at 4 °C in the dark and used within 3 days.

Ligand-binding assays using FRET. Fluorescent measurements of sterol binding to the Upc2 LBD were based on FRET between the Trp residue and bound DHE using the methods previously reported[11]. The DOPC/DHE liposomes in a molar ratio of 90:10 with a total concentration of 0.65 mM were prepared using a buffer composed of 50 mM HEPES–NaOH pH 7.2, and 120 mM potassium acetate. The 2 ml of DOPC/DHE liposomes were placed in a square quartz cell and continuously stirred with a small magnetic bar at ambient temperature. The Upc2 LBD was injected into the sample cell containing the liposomes with a final protein concentration of 0.6 µM, and the emission spectra were recorded upon excitation at 285 nm (bandwidth 5 nm) using a spectrofluorometer (FP-6200; JASCO). DHE competition assay was performed to test the binding of other sterols. The Upc2 LBD was preloaded with fluorescent DHE by incubating Upc2 with the DOPC/DHE liposomes for 6 h on ice. The competing non-fluorescent sterols (10 µM) were added to the sample cell containing the DHE-loaded Upc2, and the emission spectra of the mixtures were recorded at several time intervals.

Isothermal titration calorimetry. The protein–protein interaction of the various Upc2 constructs with Hsp90 and Impα was analyzed by ITC using an Affinity ITC calorimeter (low volume cell 190 µl; TA instruments) at 20 °C. The NLS peptide (residues 16–48) or the α12–CT of *Cg*Upc2 (residues 906–922) were fused to the C terminus of MBP for efficient protein preparation. All proteins were prepared in the identical buffer containing 20 mM Tris-HCl pH 7.5, 150 mM NaCl. The syringe was loaded with 1 mM of the Upc2 LBD, and the cell was filled with 300 µl of 0.1 mM Hsp90 (*Cg*Hsp90 or *Sc*Hsp82/*Sc*Hsc82) or importin α. The titration curve was obtained by injecting 2 µl × 25 aliquots of the Upc2 LBD into the cell at a time interval of 300 s. The enthalpy of reaction, the binding affinity, and the stoichiometry value were calculated from the measured heat changes upon the association of the Upc2 LBD and Hsp90. The titration data were analyzed using the NanoAnalyze program (TA instruments) and fitted into an independent binding model.

Plasmid construction, yeast strains, and microscopy. The yeast strain BY4741 MATa with a proper gene knockout (ThermoFisher Scientific) was used for cell imaging. The various Upc2 constructs were cloned into the pRS413MET-GFP vector. The yeast cells with *upc2Δ ecm22Δ*, *hsc82Δ*, *hsp82Δ* or wild type were transformed with the plasmids encoding various Upc2 alleles. Yeast cells expressing the appropriate alleles were grown to an OD_{600} of 0.4–0.6 in a Hartwell's complete medium without histidine. Cells were grown in the medium supplemented with 4 μg ml^{-1} of fluconazole or 5 mM ergosterol. The cells were collected and washed twice with PBS and resuspended in the selection medium for microscopic observation. Live-cell imaging was performed on an Eclipse Ti fluorescence microscope (Nikon) equipped with a fluorescein isothiocyanate filter, and the images were captured with an Andor ixon EMCCD camera. The green fluorescence of GFP–Upc2 constructs was imaged with 8 s exposure. The images of yeast cells were processed using the software ImageJ.

Western blot. The genes encoding the *Sc*Upc2 LBD (residues 598–913) and the *Sc*Hsc82 with the C-terminal 2HA-tag were cloned pRS413MET-GFP and pRS416MET, respectively. The *hsc82Δ* knockout cells of *S. cerevisiae* (BY4741, MATa his3*Δ1 leu2Δ0 met15Δ0 ura3Δ0 hsc82Δ*) were co-transformed with the plasmids encoding GFP–*Sc*Upc2 LBD and *Sc*Hsc82–HA. The yeast cells were grown to the OD_{600} of 1.5 in the minimal medium supplemented with 4 μg ml^{-1} of fluconazole or 5 mM ergosterol for 12 h. The yeast cells were harvested by centrifugation at 3,000*g*. One hundred milligrams of cells were resuspended and lysed in 500 μl of Y-PER Yeast Protein Extraction Reagent (ThermoFisher Scientific #78991) containing protease inhibitors (Pierce, A32955). The mixture was agitated at room temperature for 20 min. The cell debris was pelleted by centrifugation at 14,000*g* for 10 min. The supernatant was incubated with 20 μl of anti-HA agarose beads (Pierce, 26180) in a spin column with gentle mixing at 4 °C for 6 h. Then, the beads in the column were washed three times with 0.5 ml of TBS-T (Tris-buffered saline, 0.1% Tween 20) solution. Then, the beads suspended in 75 μl of wash buffer were added with 25 μl of sample buffer for SDS-PAGE. For the Western blot, the proteins in the SDS-PAGE gel were transferred to a PVDF membrane. GFP monoclonal mouse IgG (ThermoFisher Scientific, #MA5-15256) was used for a primary antibody with a dilution ratio of 1:3,000. The horseradish peroxidase (HRP)-coupled rabbit anti-mouse IgG (Invitrogen #VH309358) was used for the secondary antibody with a dilution ratio of 1:5,000. The *Sc*Hsc82 was detected by using an HA-tag polyclonal antibody coupled with HRP (Invitrogen, #PA1-29751) with a dilution ratio of 1:3,000. The chromogenic detection of horseradish peroxidase activity of the secondary antibody was done using CN/DAB substrate, and the blot was imaged by Azure c300 gel imaging system.

Measurement of transcription activity. pRS413-*ERG2-lacZ* was an *ERG2-lacZ* reporter made by subcloning an *ERG2* promoter, *lacZ* DNA, into the multiple cloning sites of the pRS413MET vector as previously reported[11]. pRS413-*ERG2-lacZ* and the YCplac33-*UPC2* construct were co-transformed to the *upc2Δ ecm22Δ* strain. Five milliliters of yeast cells were grown to an OD_{600} of 1, and the transcriptional activity of *Sc*Upc2 was measured using a yeast β-galactosidase assay kit (ThermoFisher Scientific, #75768).

Sterol quantification of yeast cells. Total cellular sterols of the yeast cells were extracted and quantified using the method previously described[11]. In brief, the *upc2Δ ecm22Δ* yeast cells transformed with various Upc2 alleles were grown in 50 ml Hartwell's complete media for 16 h at 30 °C. The yeast cells were harvested by centrifugation at 2,700 r.p.m. for 5 min. The harvested cells were quantified by OD_{600} of the cultures, and equal amounts of cells were used for sterol extraction. Three milliliters of 25% alcoholic KOH solution was added to the yeast pellet and vortexed for 1 min. Cell suspensions in glass tubes were incubated at 85 °C for 1 h, and the tubes were cooled down to room temperature. Sterols were extracted to *n*-heptane by adding 1 ml distilled water and 3 ml *n*-heptane followed by vortexing for 3 min. The heptane layer containing sterol was pooled for quantification using a NanoDrop 1000 Spectrophotometer (ThermoFisher Scientific). The presence of ergosterol and DHE in the extracted sample showed the absorbance spectrum with a characteristic four-peak curve.

Fluconazole susceptibility test. Fluconazole susceptibility testing was performed by introducing YCplac33 plasmids containing the full expression cassette of the wild-type or mutant *Sc*UPC2 into the yeast *upc2Δ ecm22Δ* strain. The transformed cells were grown at 30 °C until the cell density reached to OD_{600} of 1. The serial dilutions of cells (1/3, 1/9, 1/27, and 1/81) were spotted on the minimal medium agar plates containing fluconazole and incubated for 36 h.

Reporting summary. Further information on research design is available in the Nature Research Reporting Summary linked to this article.

Data availability

Coordinates and structure factors for the reported crystal structures have been deposited in the PDB with the accession codes 7VPR (*Cg*Upc2-ergosterol), 7VPU (*Lt*Upc2-ergosterol), 7XB5 (*Sc*Upc2-T4L), 7VPS (apo *Cg*Impα), and 7VPT (*Cg*Impα-Upc2 NLS). All structures cited in this publication are available under their respective PDB accession codes. Other data supporting the findings of this work are provided within the manuscript and its related source data. Source data are provided with this paper.

References

36. Sheffield, P., Garrard, S. & Derewenda, Z. Overcoming expression and purification problems of RhoGDI using a family of 'parallel' expression vectors. *Protein Expr. Purif.* **15**, 34–39 (1999).
37. Liebschner, D. et al. Macromolecular structure determination using X-rays, neutrons and electrons: recent developments in Phenix. *Acta Crystallogr D Struct. Biol.* **75**, 861–877 (2019).

Acknowledgements

This research was supported by a grant from National Research Foundation of Korea (NRF) by the Ministry of Education, Science and Technology (grant no. 2019R1A2C1085530 to Y.J.I.) and by a grant from the Korea Health Technology R&D Project through the Korea Health Industry Development Institute (KHIDI), funded by the Ministry of Health & Welfare, Republic of Korea (grant no. HI20C0079 to Y.J.I.).

Author contributions

Y.J.I. and L.T. designed the project. L.T., B.J., L.C, and H.Y. cloned the genes, purified and crystallized recombinant proteins. L.T. and L.C. performed the ligand-binding assays and yeast cell biology experiments. H.Y., L.T., and Y.J.I. collected and analyzed the X-ray data. G.K. analyzed the biochemical data. Y.J.I. wrote the manuscript. All authors discussed the results and approved the manuscript.

Competing interests

The authors declare no competing interests.

Additional information

Extended data is available for this paper at https://doi.org/10.1038/s41589-022-01117-0.

Supplementary information The online version contains supplementary material available at https://doi.org/10.1038/s41589-022-01117-0.

Correspondence and requests for materials should be addressed to Young Jun Im.

Peer review information *Nature Chemical Biology* thanks Anders Näär, David Rogers and the other, anonymous, reviewer(s) for their contribution to the peer review of this work.

Reprints and permissions information is available at www.nature.com/reprints.

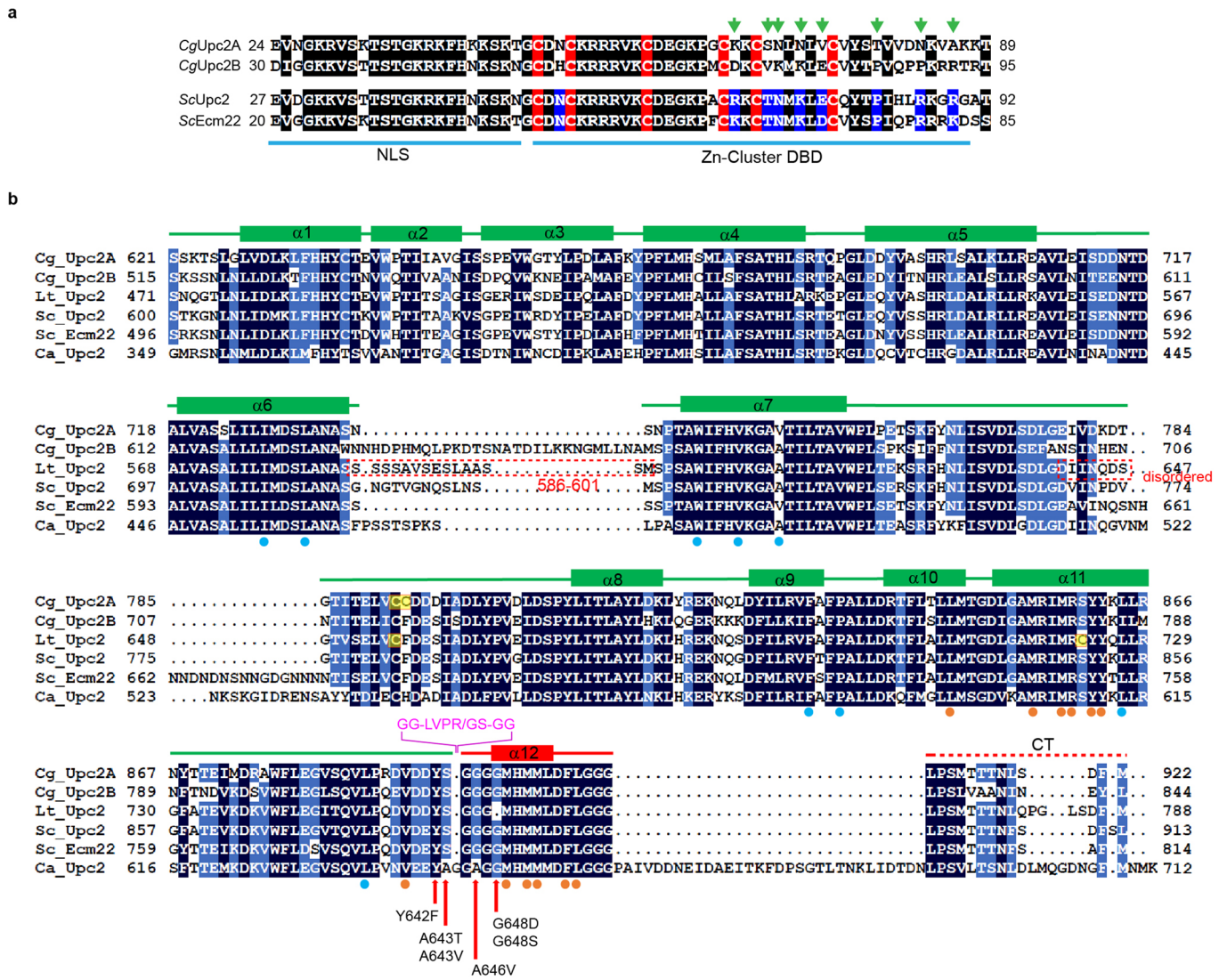

Extended Data Fig. 1 | Sequence alignments of Upc2 homologs. a, The sequence alignments of the N-terminal regions of Upc2 homologs from *C. glabrata* and *S. cerevisiae*. The six cysteines coordinating Zinc clusters were colored in red. The variable residues in the DBDs of *Cg*Upc2 homologs were indicated by green arrows. The corresponding residues in *Sc*Upc2 and *Sc*Ecm22 are well conserved and colored in blue. **b**, The sequence alignments of Upc2 LBDs. The secondary structure elements were based on the structure of *Cg*Upc2. The helix α12 and the C-terminal tail are shown in red. The disordered region in the crystal structure is indicated with dotted lines and boxes. The residues composing the hydrophobic sterol-binding pocket are marked with filled circles. The residues contacting the hydrocarbon rings of sterols are shown in orange circles, and the residues contacting the hydrocarbon side chain in blue circles, respectively. The constitutive active mutations of Upc2 identified in the clinical isolates of azole-resistant *C. albicans*[18] were indicated by red arrows. The insertion mutation of the thrombin recognition sequence was indicated by purple letters.

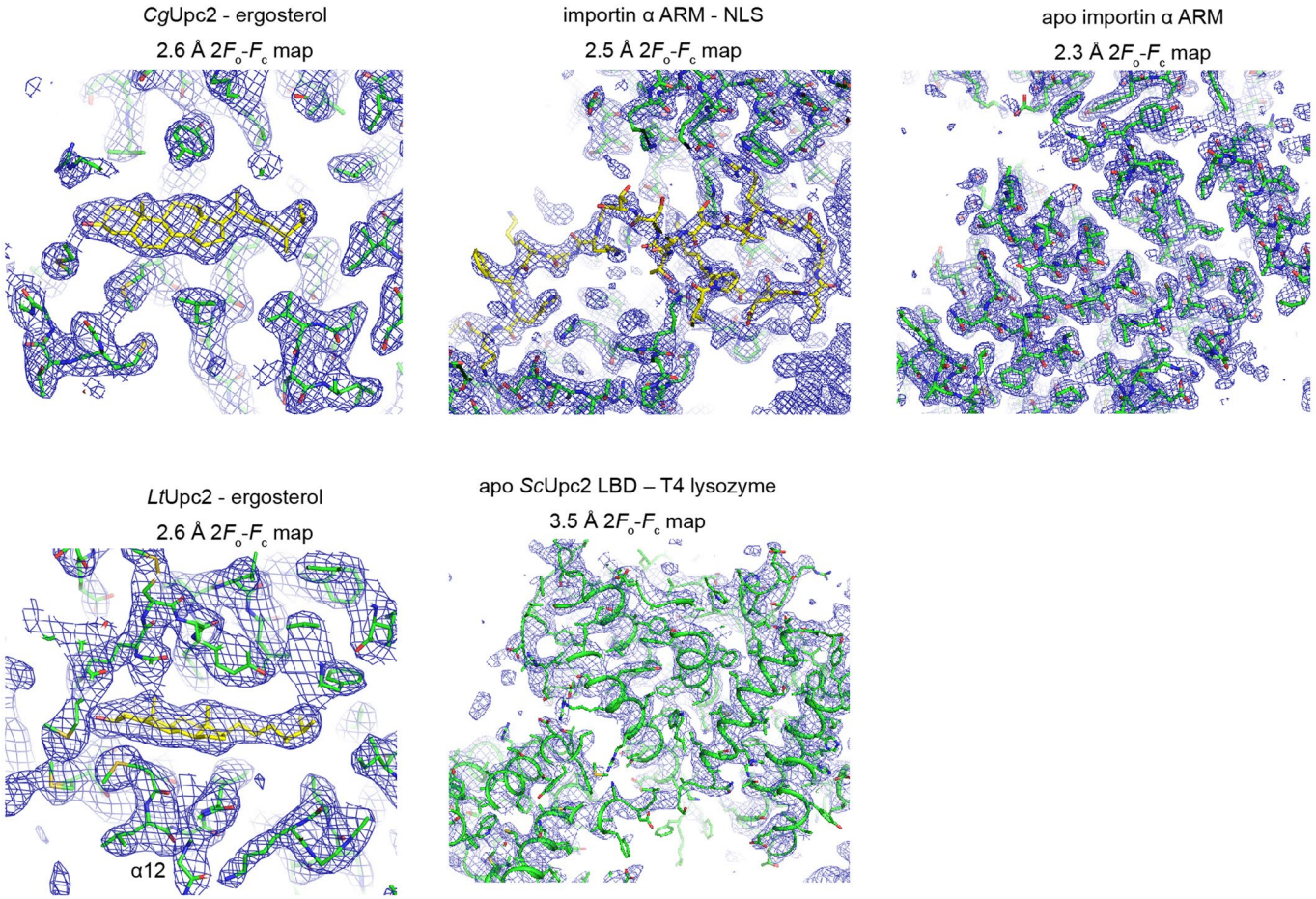

Extended Data Fig. 2 | The $2F_o$-F_c electron density maps of the crystal structures. The final models were superimposed into the electron densities.

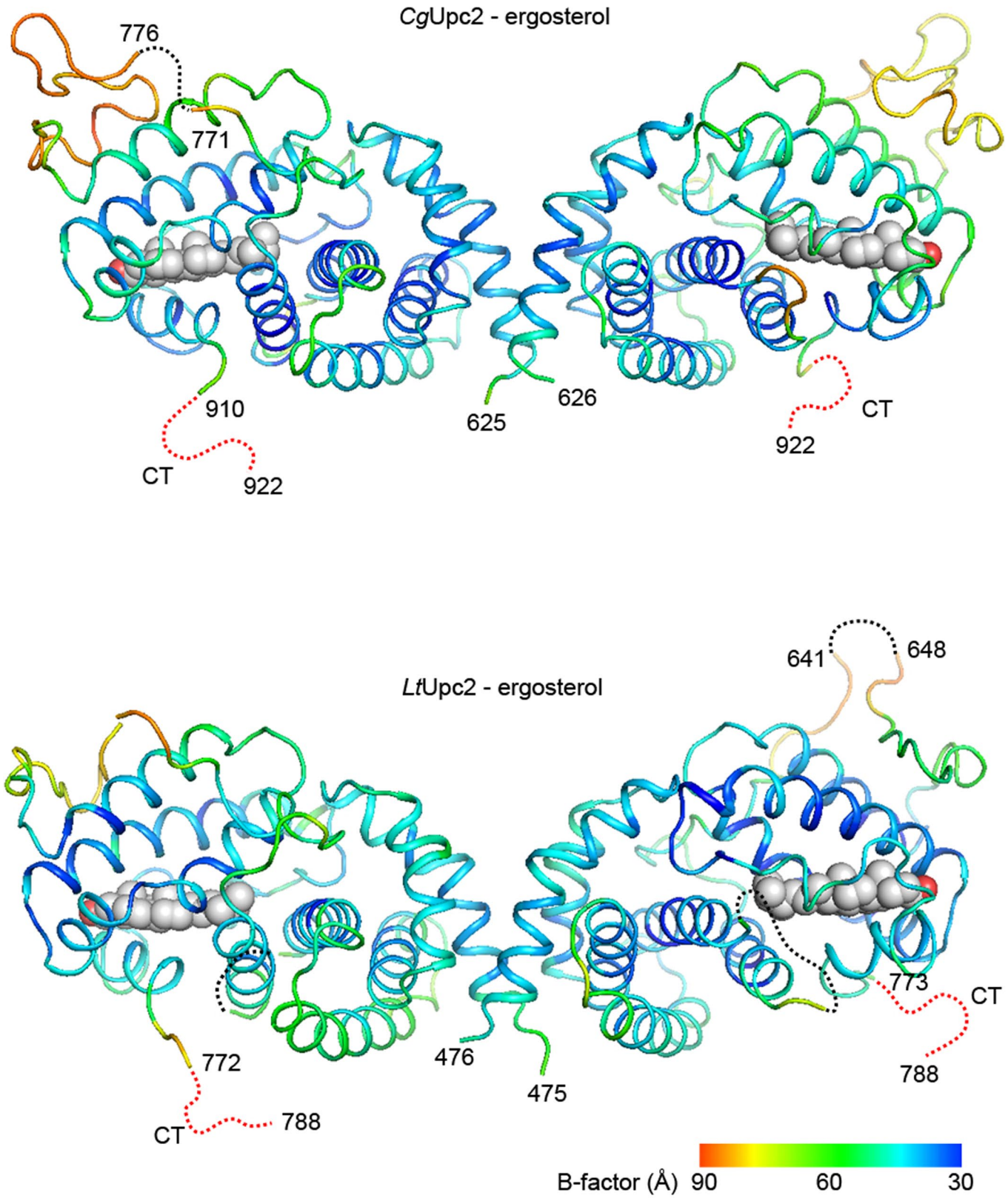

Extended Data Fig. 3 | B-factor representation of the *Cg* and *Lt*Upc2 LBDs. The disordered regions which were not included in the structural models were indicated by dotted lines.

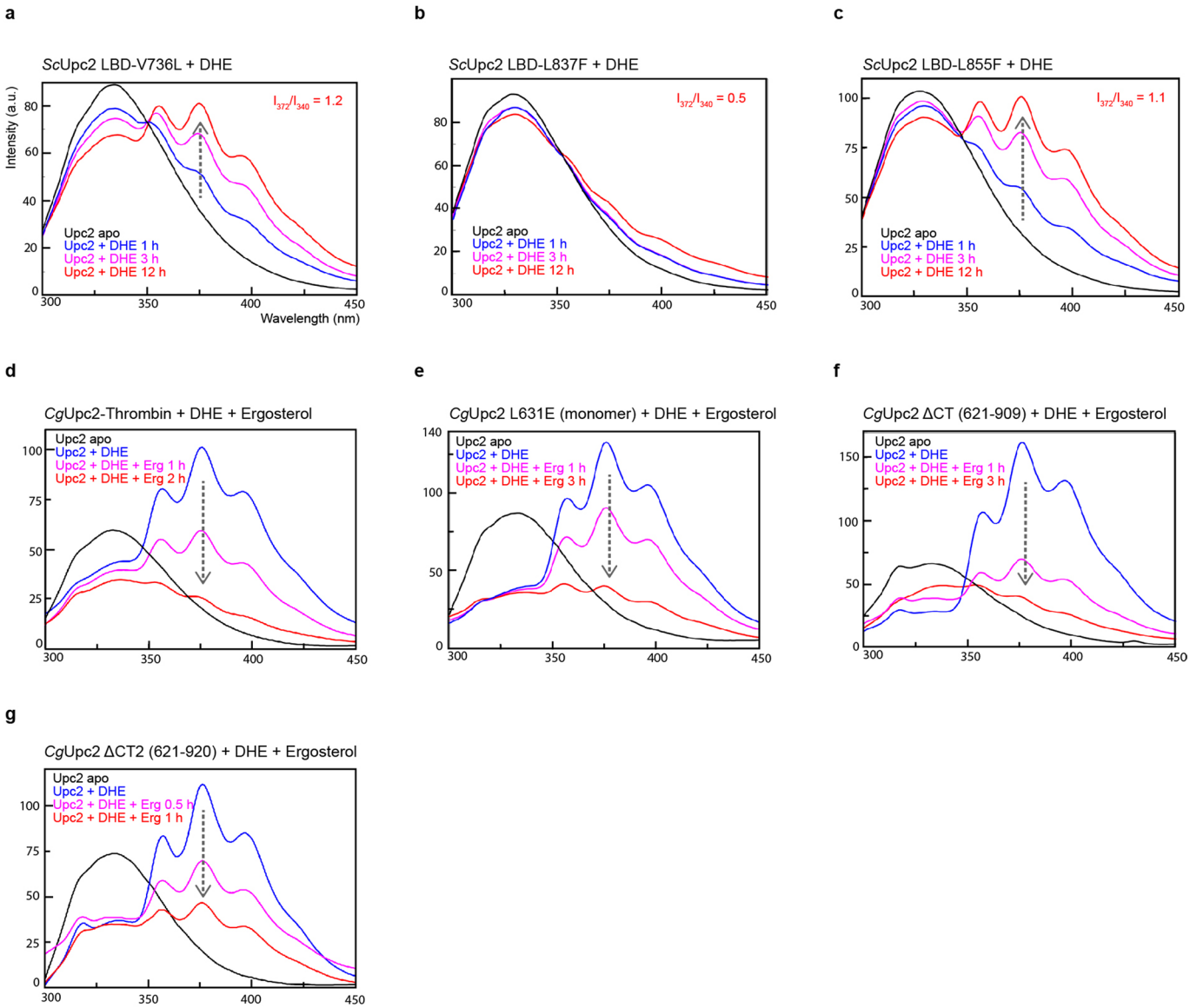

Extended Data Fig. 4 | Sterol-binding assay of *Sc*Upc2 and *Cg*Upc2 constructs. a-c, The DHE binding assays of *Sc*Upc2 LBD mutants. **d-g**, Ergosterol-competition assay of *Cg*Upc2 constructs. The competing ergosterol was added to the Upc2 LBD preloaded with DHE. The spectral measurements were repeated two times, and the representative data were shown.

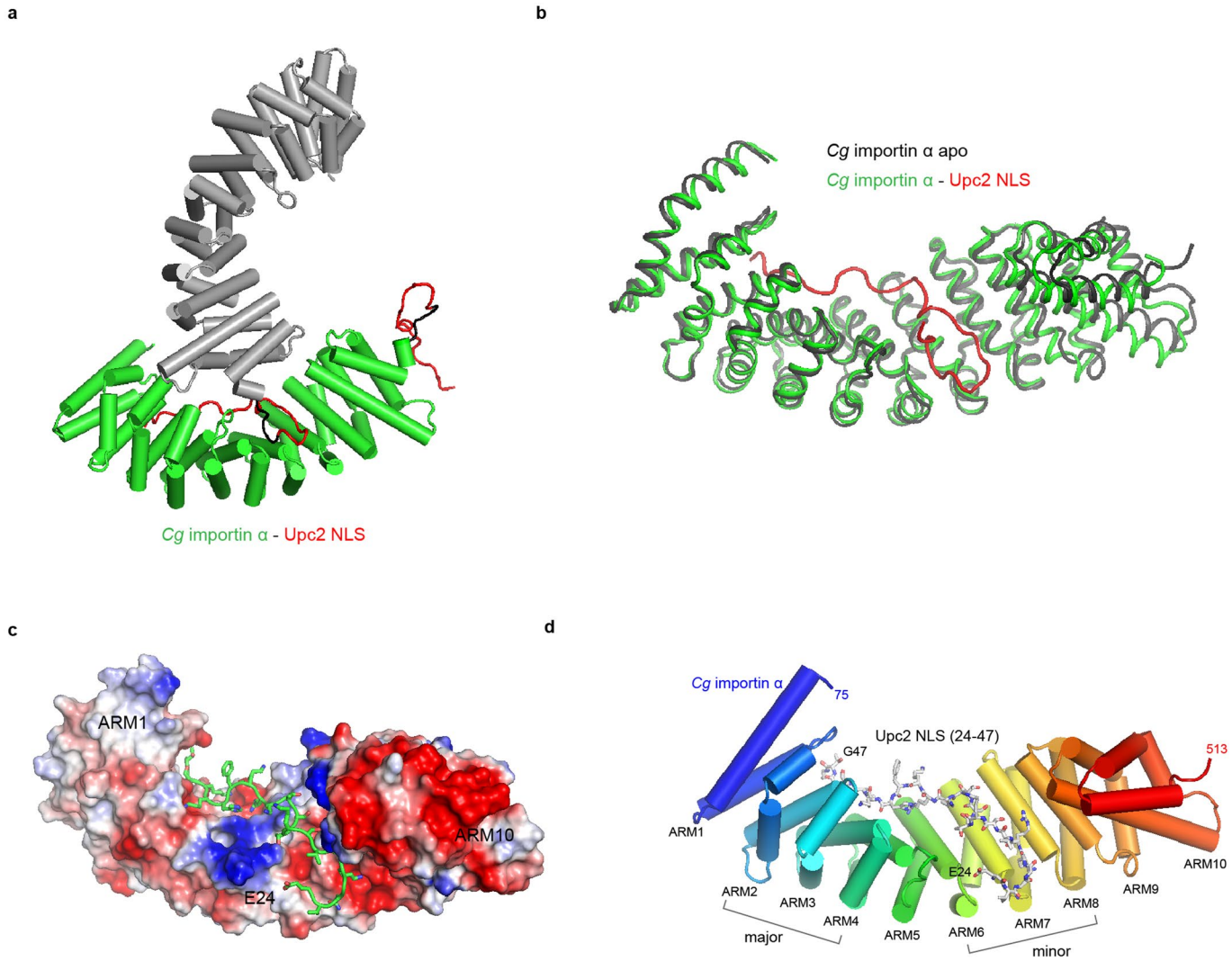

Extended Data Fig. 5 | Structure of *Cg*Impα-Upc2 NLS complex. a, Association of the C-terminal NLS sequence from a neighboring molecule to the importin α in a head-to-tail fashion in the crystal lattice. **b**, Structural comparison of apo importin α and the NLS-bound importin α. The Upc2 NLS sequence (residues 24-47) fused to the C-terminus of importin α is colored in red. **c**, Surface representation of the *Cg*Impα–Upc2 NLS complex. The electrostatic surface was shown for *Cg*Impα ARM. **d**, Overall structure of the *Cg*Impα–Upc2 NLS complex. The ARM domain of *Cg*Impα is colored in blue to red from the N- to C- terminus. The Upc2 NLS is shown in stick models.

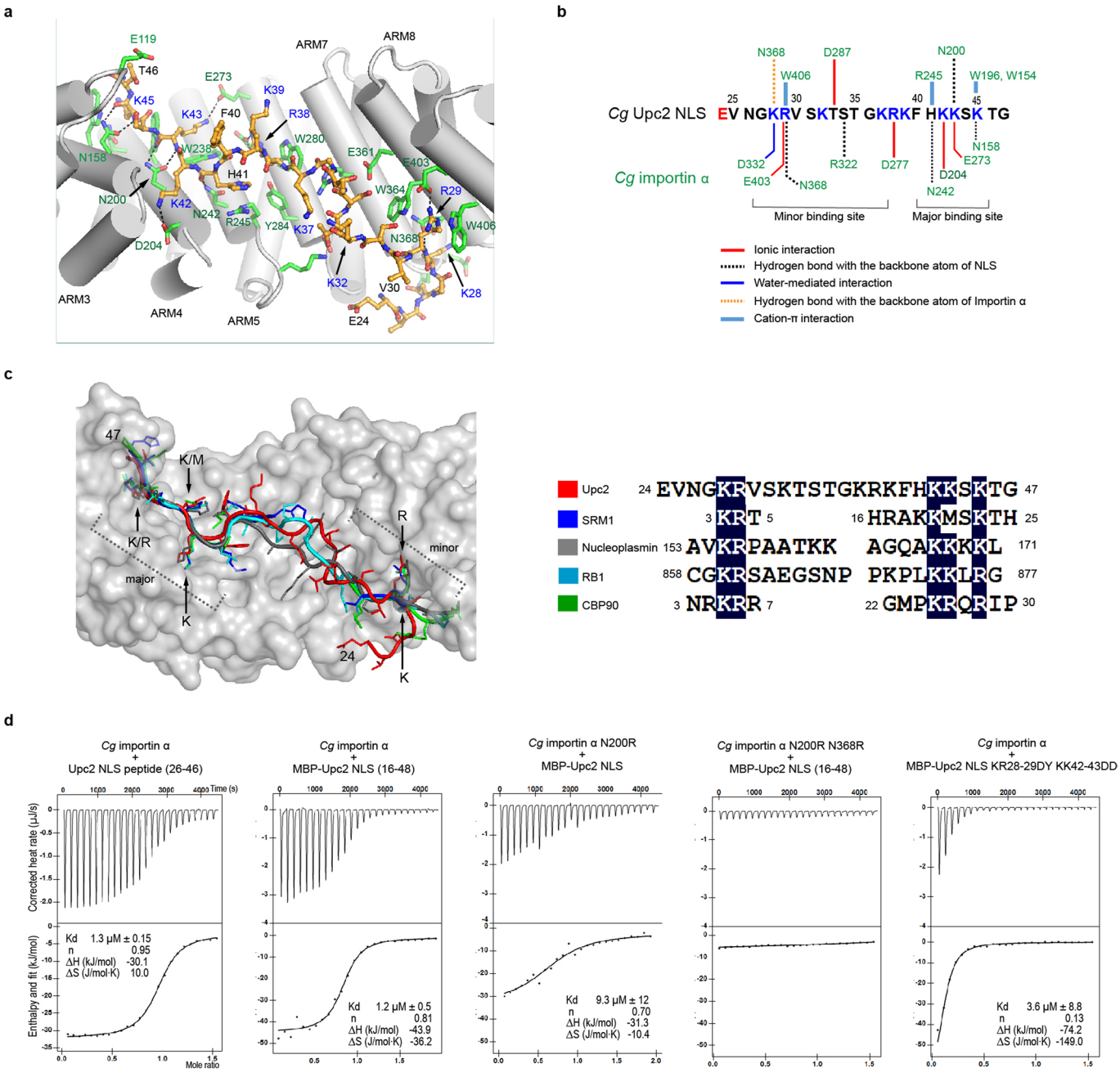

Extended Data Fig. 6 | The Upc2 NLS bind site of *Cg*Impα. a, Detailed view of the *Cg*Impα–Upc2 NLS binding interface. The Upc2 NLS is shown in orange and the importin α residues in green. Hydrogen bonds and salt bridges are shown in dotted lines. **b**, The schematic representation of the *Cg*Impα–Upc2 NLS interaction. The non-covalent interactions between Impα and Upc2 NLS were summarized in a schematic representation. **c**, Structural comparison of the NLS-binding modes of the various Impα–cargo complexes. The bound NLS sequences were shown for Upc2 (this study), SRM1 (PDB: 4OIH), Nucleoplasmin (PDB: 1EE5), RB1 (PDB: 1PJM), and CBP90 (PDB: 3UKY). **d**, ITC analysis of the importin α and Upc2 NLS interaction. The *Cg*Impα in the cell was titrated with the Upc2 NLS peptide or MBP-Upc2 NLS in the syringe. The ITC measurements were repeated two times, and one representative data was shown for each construct.

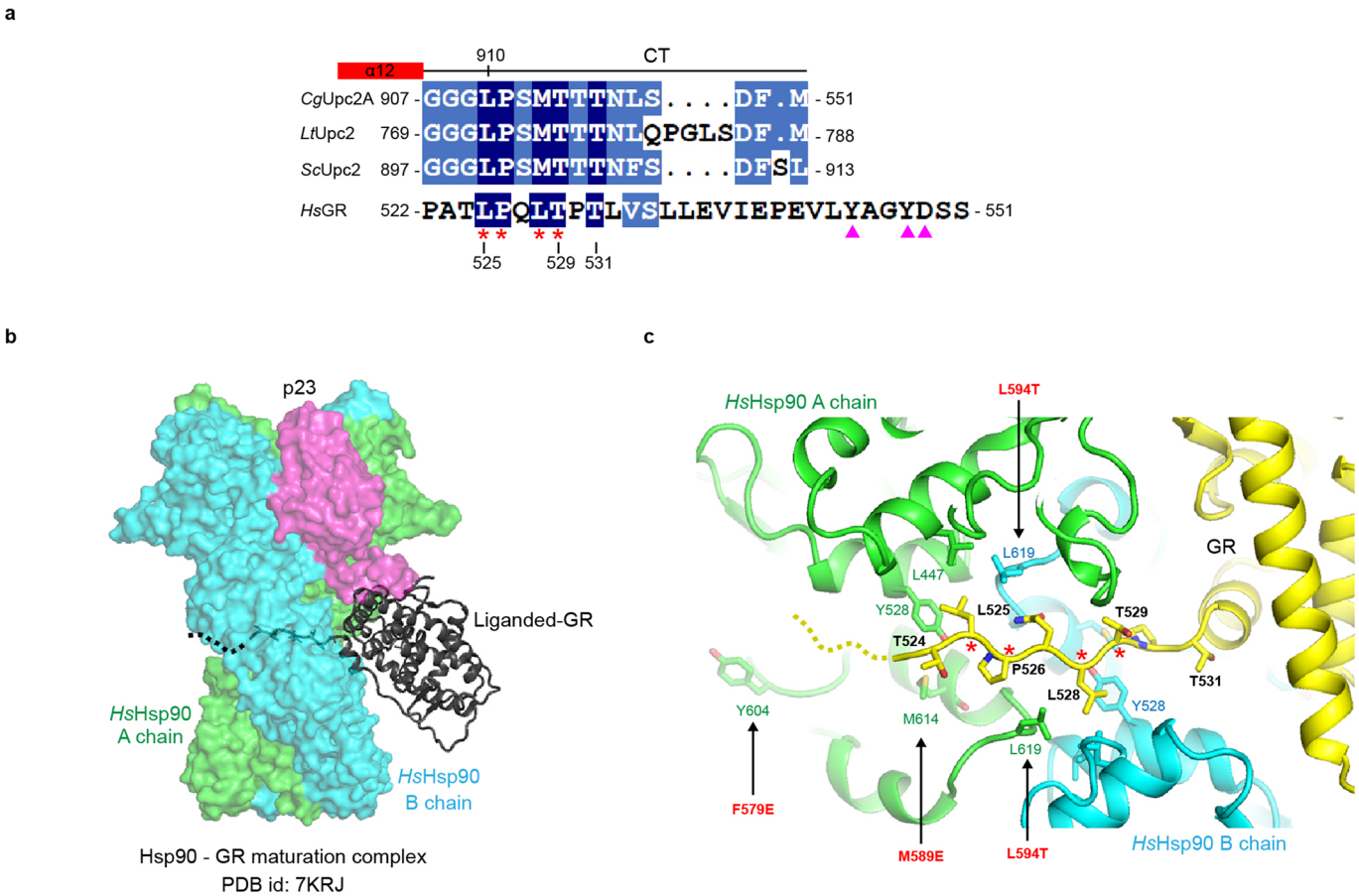

Extended Data Fig. 7 | Conservation of a client binding mode of Hsp90 on *Cg*Upc2 and GR. a, The sequence alignments of the CT regions of Upc2 homologs with the Hsp90-binding region of human GR. The conserved Hsp90-binding residues in the client proteins were indicated by blue shades. Asterisks indicate the GR residues interacting with *Hs*Hsp90 in the maturation complex[28], and purple triangles indicate the residues interacting with *Hs*Hsp90 in the loading complex[29]. **b**, Structure of *Hs*Hsp90–GR maturation complex. The sterol-bound GR is shown in black ribbons. The N-terminal extended loop binds to the lumen of the *Hs*Hsp90 homodimer. **c**, The GR-binding site of Hsp90. The red labels indicate the mutated residues at the equivalent positions in *Cg*Hsp90.

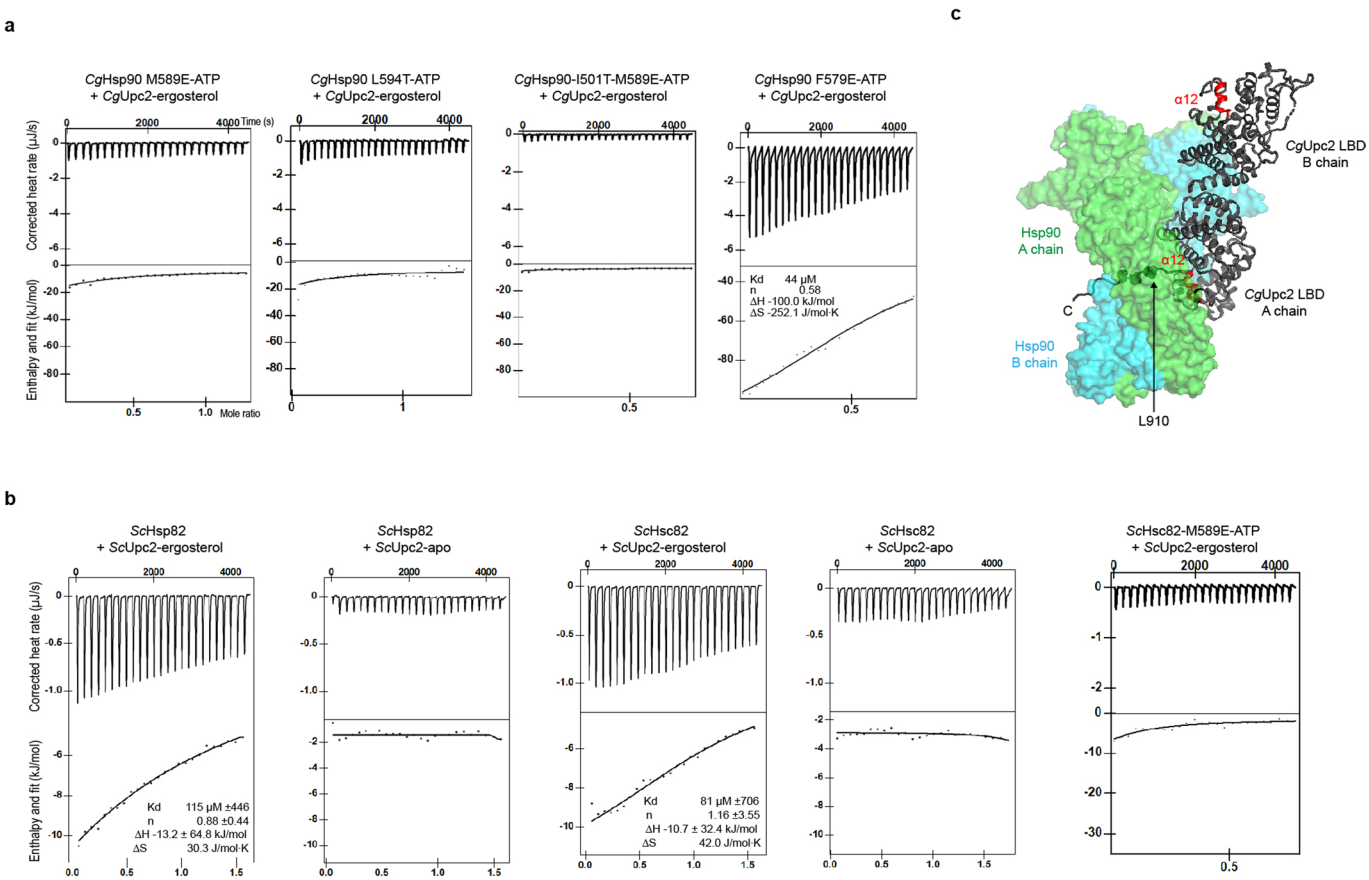

Extended Data Fig. 8 | ITC analysis of Hsp90 - Upc2 interaction. a, ITC analysis of L594T and M589E mutants of *Cg*Hsp90 for *Cg*Upc2 binding. **b**, The two Hsp90 isoforms (Hsc82 and Hsp82) of *S. cerevisiae* were tested for the ergosterol-dependent interaction of the *Sc*Upc2 LBD by ITC. M589E mutation in *Sc*Hsc82 abolished the interaction with the *Sc*Upc2 LBD-ergosterol. The ITC measurement was repeated two times, and one representative data was shown for each construct (Supplementary Fig. 4). **c**, Structural model of the *Cg*Hsp90 – *Cg*Upc2 complex. The human Hsp90 dimer in the maturation complex was used for the template of *Cg*Hsp90. The extended loop residues of GR interacting with Hsp90 were replaced by the CT sequence of *Cg*Upc2. The dimeric structure of *Cg*Upc2 LBD was manually located to the N-terminus of the modeled CT in an orientation with minimum steric clashes between Hsp90 and Upc2.

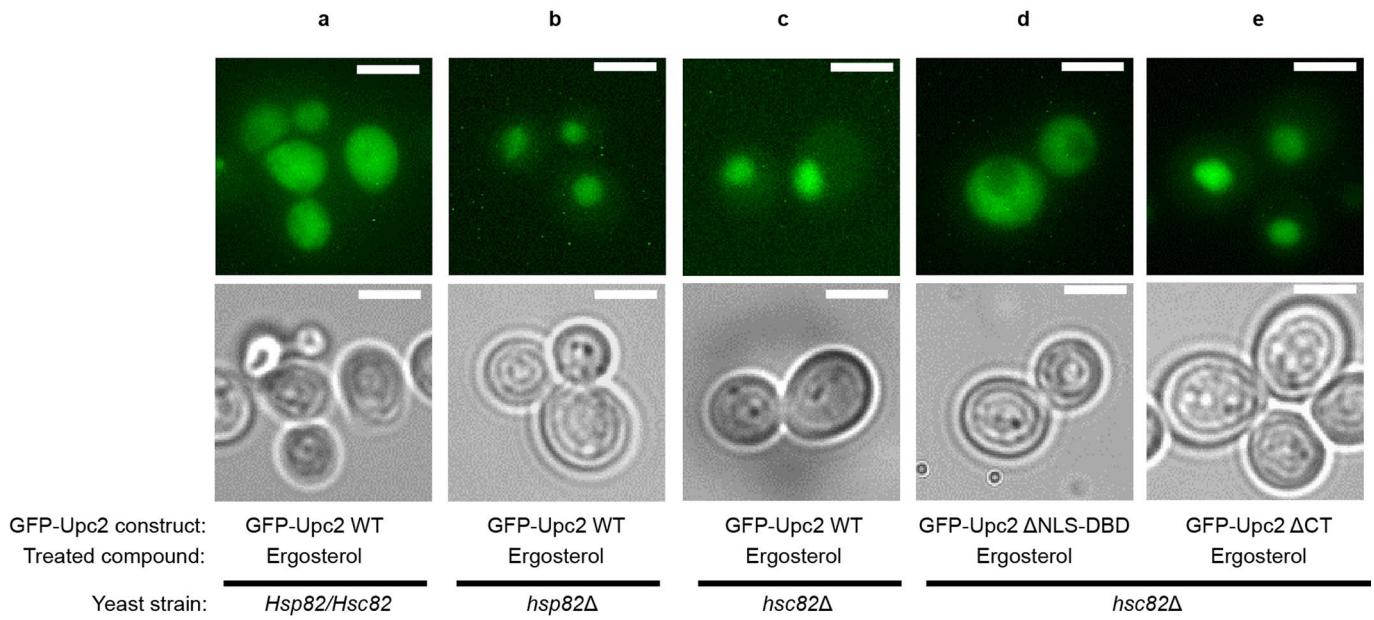

Extended Data Fig. 9 | Hsp90-dependent localization of Upc2. a-e, To test the significance of *Sc*Hsp90 isoforms (Hsc82 and Hsp82) on Upc2 regulation, the localization of GFP-Upc2 constructs was examined in the yeast knockout strains (*hsc82Δ* or *hsp82Δ*) grown in the presence of ergosterol. The microscopic imaging of the yeast cells was repeated two times with consistent results. More than 300 cells were examined, and the cell images representing higher than 80% of the cell population were shown in the panels. Scale bar, 3 μm.

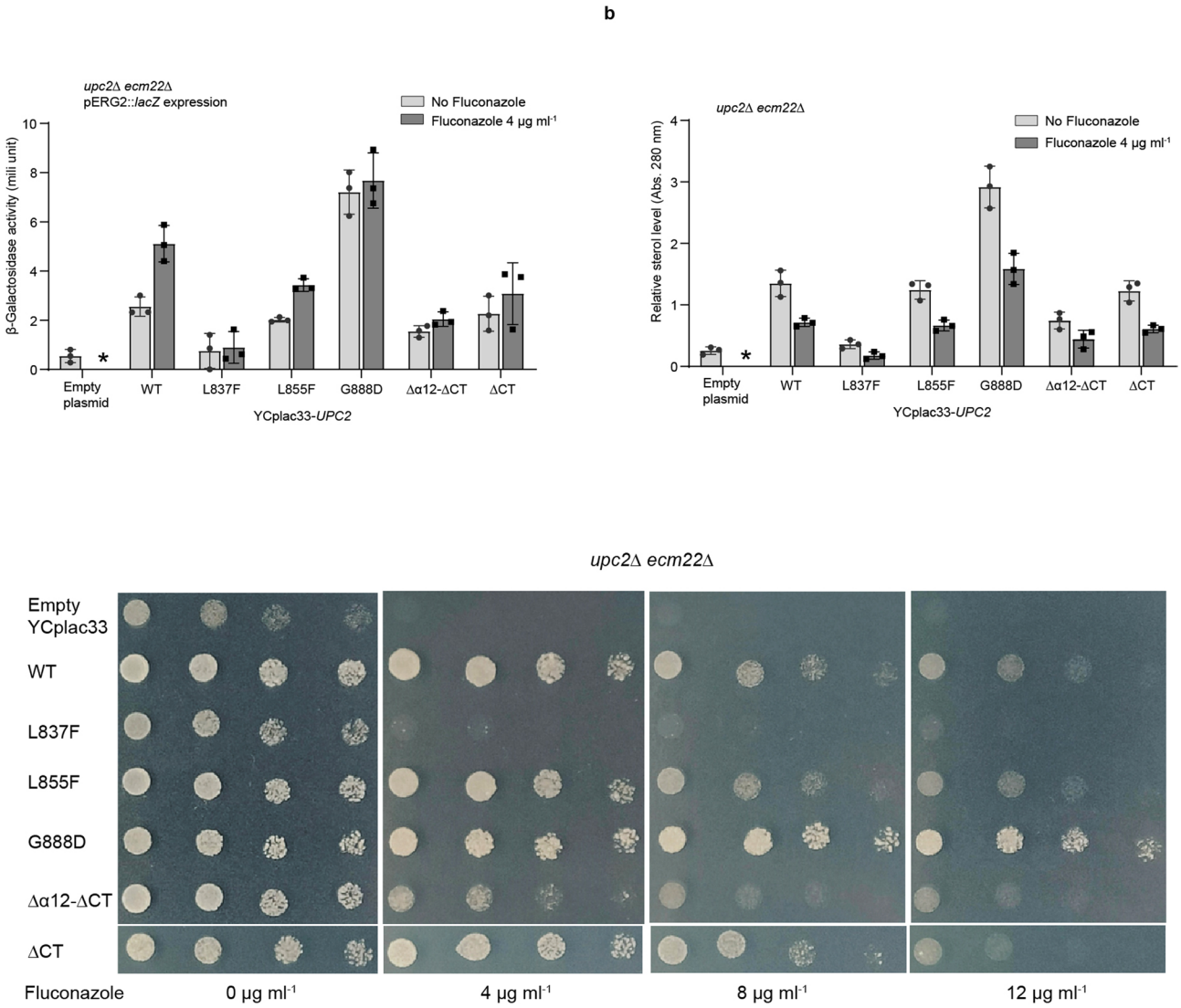

Extended Data Fig. 10 | Transcriptional control of ergosterol level and azole resistance. a, Transcriptional activity of Upc2. *ERG2-lacZ* reporters were used to determine the contribution of each Upc2 construct to the regulation of *ERG2* promotor. The assay values represent the average of three independent experiments. All error bars indicate standard deviations. The individual data points for three-repeating experiments were overlaid in dots for each bar graph. **b**, Quantification of total ergosterol in yeast cells. Yeast *upc2Δ ecm22Δ* strain transformed with the YCplac33 plasmids containing full cassette of various *UPC2* alleles were analyzed for their cellular ergosterol levels. Each data point is the average of three measurements. The error bars indicate standard deviations. The individual data points for three-repeating experiments were overlaid in dots for each bar graph. **c**, Susceptibilities to fluconazole of the *upc2Δ ecm22Δ* yeast strain expressing wild-type or mutant UPC2 alleles. The strains were initially grown without fluconazole, and the dilution series of 1/3, 1/9, 1/27, 1/81 were spotted on the agar plates containing fluconazole and incubated for 36 h.